Sensing and imaging using laser feedback interferometry with quantum cascade lasers

A. D. $_{Rakić}$ (iD), T. Taimre (iD), K. Bertling (iD), Y. L. Lim (iD), P. Dean (iD), A. Valavanis (iD), and D. Indjin (iD)

COLLECTIONS

EP   This paper was selected as an Editor's Pick

View Online   Export Citation   CrossMark

ARTICLES YOU MAY BE INTERESTED IN

On-chip mid-infrared and THz frequency combs for spectroscopy
Applied Physics Letters **114**, 150401 (2019); https://doi.org/10.1063/1.5097933

Applied Physics Reviews
Now accepting original research

2017 Journal
Impact Factor:
12.894

Sensing and imaging using laser feedback interferometry with quantum cascade lasers EP

View Online   Export Citation   CrossMark

A. D. Rakić,[1,a)] (iD) T. Taimre,[2] (iD) K. Bertling,[1] (iD) Y. L. Lim,[1] (iD) P. Dean,[3] (iD) A. Valavanis,[3] (iD) and D. Indjin[3] (iD)

AFFILIATIONS

[1]School of Information Technology and Electrical Engineering, The University of Queensland, Brisbane, QLD 4072, Australia
[2]School of Mathematics and Physics, The University of Queensland, Brisbane, QLD 4072, Australia
[3]School of Electronic and Electrical Engineering, University of Leeds, Leeds LS2 9JT, United Kingdom

[a)]a.rakic@uq.edu.au

ABSTRACT

Quantum cascade lasers (QCLs) are high-power sources of coherent radiation in the midinfrared and terahertz (THz) bands. Laser feedback interferometry (LFI) is one of the simplest coherent techniques, for which the emission source can also play the role of a highly-sensitive detector. The combination of QCLs and LFI is particularly attractive for sensing applications, notably in the THz band where it provides a high-speed high-sensitivity detection mechanism which inherently suppresses unwanted background radiation. LFI with QCLs has been demonstrated for a wide range of applications, including the measurement of internal laser characteristics, trace gas detection, materials analysis, biomedical imaging, and near-field imaging. This article provides an overview of QCLs and the LFI technique, and reviews the state of the art in LFI with sensing using QCLs.

TABLE OF CONTENTS

I. INTRODUCTION

Laser feedback interferometry (LFI), also known as self-mixing (SM) interferometry, is a compact sensing technique wherein radiation emitted from the laser interacts with an external target and is subsequently reflected back into the laser. The reinjected emission mixes with the intracavity electric field, causing small variations in the fundamental laser parameters, including the threshold gain, lasing spectrum, emitted power, and laser terminal voltage. This technique has been used for a range of sensing and imaging applications, and has been implemented with a variety of lasers. However, its distinct advantage over other coherent schemes may be realized in the mid-infrared (MIR) and terahertz (THz) regions of the electromagnetic (EM) spectrum, where quantum cascade lasers (QCLs)—unipolar devices exploiting a cascading series of intersubband transitions to achieve stimulated emission—are the radiation sources of choice. It is the high output power, low phase-noise, and stability under feedback of QCLs, combined with the high sensitivity of LFI coherent detection, that will unlock the true potential for sensing and imaging in these parts of the EM spectrum.

It has been over 25 years since the advent of an MIR QCL device[1–3] and over 15 years since the first demonstration of the QCL at THz frequencies.[4] At present, the QCL is mostly applied in the sensing domain, where the advantage of high emitted power from a QCL source is prized—in particular, at THz frequencies and in the MIR.[5–7] There are inherent advantages in interferometric (coherent) sensing—not only the intensity/amplitude, but also phase information can be captured. In imaging, this permits the concurrent registration of both amplitude and phase information.[8–13]

Laser feedback interferometry is the simplest implementation of a coherent sensing technique. It is particularly attractive when the transmitter and the detector are combined in one device. In this embodiment, the optical part of the system has a coaxial geometry through which the incident beam is transmitted and reflected from the target, with the reflected beam traversing the same optical path in reverse. The combination of a transmitter and a detector in one device implies no need for target/sample preparation, and therefore their potential for *in situ* and *in vivo* sensing and imaging with QCLs. A further distinct benefit is realized in frequency ranges where the existing detectors are not sensitive or fast enough. The interferometric signal can be obtained by monitoring the feedback-caused voltage variations across the laser terminals caused by the SM effect in the QCL; thus, the QCL itself acts as a high speed and highly sensitive detector.[14,15]

In this review, we outline the physical principles underpinning the operation of LFI sensors, the SM effect in QCLs, and review the state of the art in sensing and imaging using LFI with QCLs. We open in Sec. II by briefly outlining the operating principles of QCLs. In Sec. III, we discuss the basic theory underpinning LFI and the fundamental model for feedback in QCLs, namely the excess phase equation [equivalent to the Lang–Kobayashi (LK) model in the steady-state]. Although not covered here, the essential dynamic behavior of lasers under feedback, including QCLs, is captured in the LK model[16] and refined in more recent works (c.f. Refs. 17–20). Crucially, these models permit one to predict the behavior of the SM signal and ultimately the voltage across the laser terminals.[21] We devote a significant portion of our review to applications

of sensors using the SM effect in QCLs. In Sec. IV, we divide applications into two parts: (i) those related to internal laser characteristics such as the measurement of linewidth, linewidth enhancement factor (LEF, Henry's α), emission spectrum, and phase-noise and (ii) those related to measurements external to the laser, such as displacement sensing including ablation and multiple target displacement; materials analysis including gas detection, organic materials analysis, and measurement of the distribution of free carriers; and imaging including near-field imaging and coherent imaging for biomedical applications. We conclude by summing up the current state of the art and discussing the road ahead for LFI with QCLs in Sec. V, with particular focus on the most attractive and promising directions, including biomedical and high-speed sensing and imaging.

II. QUANTUM CASCADE LASERS: PRINCIPLES OF OPERATION AND MODELING

Quantum cascade lasers are unipolar devices which exploit intersubband transitions in the conduction band of a semiconductor multiple-quantum-well heterostructure for radiation amplification.[3,22–24] A photograph of a typical THz QCL, indium mounted on a gold-plated copper carrier with gold-wire bonding to the QCL electrical contacts, is shown in Fig. 1(a). In an applied electric field, electrons stream down a "potential staircase," sequentially emitting a low-energy photon at each of its "steps"—a series of multiquantum well structures comprising a period of the QCL structure, repeated several tens or
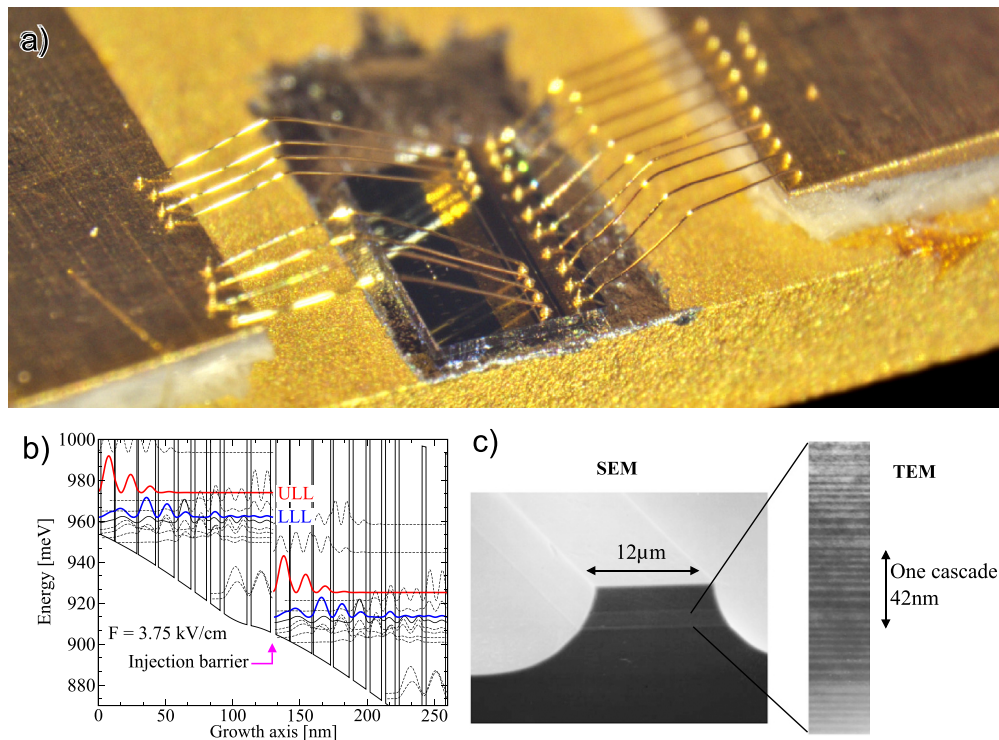
FIG. 1. (a) A photograph of a typical THz QCL. (b) Band structure and electron wavefunction moduli squared of a single-mode bound-to-continuum (BTC) THz QCL emitting at 2.59 THz. The upper lasing level (ULL) and the lower lasing level (LLL) are indicated (solid lines) together with miniband extraction states (dashed lines), under an applied electric field of 3.75 kV/cm. (c) Scanning electron microscopy (SEM) and transmission electron microscopy (TEM) images of a MIR QCL.[25] Reproduced with permission from G. Purvis, III-Vs Rev. **19**(8), 20–25 (2006). Copyright 2006 Elsevier.

hundreds of times, designed to create population inversion between a pair of excited subbands.[1] Figure 1(b) shows the band structure and electron wavefunction moduli squared of a single-mode bound-to-continuum (BTC) THz QCL emitting at 2.59 THz under an applied electric field of 3.75 kV/cm. Thus, each electron injected above the threshold may generate a photon per step—it is this cascading process which underpins the intrinsic high-power capability of QCLs.[3,10,22] The design of the QCL structure is achieved by "band structure engineering"; that is, tailoring the quantum well and barrier thicknesses and barrier heights within the heterostructure to control the fundamental properties (energy levels, band-offset, carrier scattering rates, optical dipole matrix elements, and tunneling times).[3,22]

The theoretical basis of the QCL lies in the work of Esaki and Tsu in 1970[26] on superlattices and the proposal by Kazarinov and Suris in 1971[27] of using intersubband transitions for radiation amplification, with the first working QCL demonstrated at Bell Labs in 1994.[1] Unlike conventional interband lasers, for which the emission wavelength depends on the material bandgap, in QCLs the emission wavelength is primarily determined by the energy spacing of lasing sub-bands and not the bandgap of the material. Consequently, one can choose a reliable semiconductor material system,[154] tailoring wavelengths over a wide range of values ($\sim$1–100 THz or $\sim$3–300 μm, excluding Reststrahlen bands which are dependent on the semiconductor material system[28]) by varying layer thicknesses.[1,3,4,22] Furthermore, gain in interband lasers is strongly temperature dependent, whereas in QCLs it depends indirectly on the temperature.[3,10]

Due to the precision required to manufacture the quantum-engineered heterostructure, QCL devices are typically grown via molecular beam epitaxy or metalorganic vapor phase epitaxy.[1,29] Figure 1(c) shows scanning electron microscopy (SEM) and transmission electron microscopy (TEM) images of an MIR QCL, in which the periodic nature of the growth can be clearly seen. To date, best performance has been obtained with four semiconductor material systems:[156] GaInAs/AlInAs grown on InP substrates; GaAs/AlGaAs grown on GaAs substrates; AlSb/InAs grown on InAs substrates; and InGaAs/AlInAsSb, InGaAs/GaAsSb, or InGaAs/AlInGaAs grown on InP substrates. The choice of the material system affects the intersubband gain, the shortest possible wavelength of operation dictated by the conduction band, and the location of the Reststrahlen bands.[3,155,156]

The intrinsic (quantum noise limited) linewidth of QCLs is subkilohertz, around 500 Hz for MIR QCLs and around 100 Hz for THz QCLs.[30–34] Practical instantaneous linewidths are around 10 kHz, and on the order of tens of megahertz over longer time-scales.[10] Consequently, QCLs are high-power sources of high spectral purity (intrinsically, $Q = \lambda/\Delta\lambda = \nu/\Delta\nu$ is greater than around 10^{10}; practically, Q is greater than around 10^5 or 10^6), and therefore QCLs naturally exhibit a long coherence length. Moreover, in QCLs, the intersubband transitions exhibit ultrafast carrier dynamics, and as a consequence of the short carrier lifetime relative to the photon lifetime, the devices lack pronounced relaxation oscillations in sharp contrast to conventional interband laser diodes.[22] The dominant scattering mechanism for nonradiative intrawell transitions is electron-longitudinal optical (LO) phonon scattering, with a lifetime typically less than 1 ps. On the other hand, nonradiative interwell relaxation is dominated by a combination of electron–electron, electron impurity, interface roughness, and LO-phonon scattering of the high-energy tail of the subband electron distribution.[3,10] Furthermore, predominantly due to thermally activated LO phonon scattering between

the upper and lower laser subbands,[35] GaAs-based THz QCLs have an operating temperature ceiling of around 200 K.[36]

The predominant active region designs for QCLs are chirped superlattice, BTC, resonant phonon, and hybrids of these.[3,10,37] Due to the ultrafast intersubband carrier dynamics, achieving optical gain requires high electrical power dissipation. Consequently, the incorporation of optical waveguides into the laser cavity design is essential to minimize electrical dissipation.[37] For MIR QCLs, the waveguide design is based on dielectric confinement with the use of cladding layers (on the order of the wavelength, $\sim$3–25 μm), sometimes employing single interface (i.e., surface) plasmon enhancement.[37] However, for THz QCLs, the thickness of the required cladding layers (on the order of the wavelength, $\sim$60–300 μm) now becomes prohibitively large, and so alternative waveguiding architectures are sought.[37] Prominent architectures at present are semi-insulating single metal surface-plasmon enhanced and double metal waveguides.[3,5,22,37] Waveguides are typically realized by processing into a ridge or buried heterostructure geometry.

Finally, prominent optical cavity designs are Fabry–Pérot (FP, typically formed via cleaving), distributed feedback (DFB, for control of mode selection, typically realized either via a surface or buried periodic Bragg grating), or external cavity designs (EC, enabling tuning by reflection from a diffraction grating in a Littrow configuration).[37] Each QCL design has strengths and weaknesses, striving to strike balance with trade-offs in injection efficiency, extraction efficiency, gain coefficient, and overlap of the optical mode in the waveguide with the active region; the design of QCLs remains an active area of research.

Presently, a large number of QCLs have been realized, operating in a continuous wave (cw) mode or pulsed mode (see Fig. 2). Midinfrared QCLs have been demonstrated with multi-Watt output power and room temperature cw operation.[5,39] Terahertz QCLs have been demonstrated with >2.4 W output power in pulsed mode[40] and >130 mW in cw,[41] at temperatures up to 199.5 K in pulsed mode and 129 K in cw operation.[3,5,11]

Physical (*ab initio*) models are typically used to study the quasi-static characteristics of QCLs, such as the gain profile or light–current (L–I) characteristics.[42] There are four main physical/complete modeling
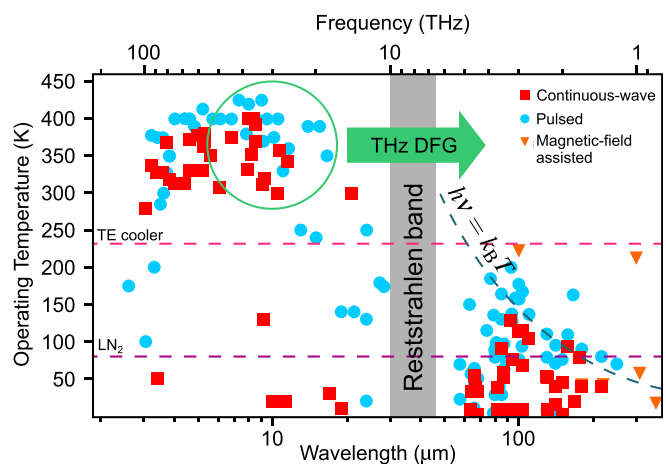

FIG. 2. Emission wavelength/frequency vs operating temperature of QCLs. The green arrow refers to creating THz emission by means of difference frequency generation (DFG) from MIR QCLs. Data from Refs. 3, 5, and 38.

frameworks employed in theoretical studies of QCLs. (I) Rate equation (RE) methods, for which the (time-independent, but spatially dependent along the growth axis) Schrödinger equation (which takes the total crystal potential as an input and outputs the wavefunctions) is solved self-consistently with the Poisson equation (which takes the confinement potential as input, itself being dependent on the charge distribution which depends on the wavefunctions and outputs electric potential). Typically, this is an iterative numerical procedure, and the relevant equations are discretized to obtain tridiagonal systems of linear equations. Assumptions are made on the shape of the electron distribution function (e.g., Fermi–Dirac distribution), and that there is incoherent scattering between modules. However, this latter assumption can lead to unphysical hybridization of wavefunctions. (II) Density matrix formalism, which permits transport between modules to be modeled as a coherent tunneling process, while typically assuming incoherent scattering within quasi-steady states within a single periodic module.[43–46] (III) Nonequilibrium Green's function approach, which provides a complete quantum mechanical description of electron transport.[47–49] (IV) Monte Carlo methods, which essentially rely on a direct physical description of the device and material's parameters.[50–53] For a detailed survey of modeling approaches for QCLs, see Jirauschek and Kubis.[42]

Reduced rate equation (RRE) models are an alternative approach in which a subset of laser parameters is considered, enjoying an advantage in terms of computational efficiency. These models are frequently used to study the dynamic characteristics of QCLs, with the simple two- or three-level RRE model being commonplace.[37,54,55] Agnew et al.[17,18,20] extended this concept to a realistic RRE model for a particular BTC THz QCL by incorporating a thermal model as well as temperature- and bias-dependent coefficients obtained via a full RE model. This work highlights that the QCL structure (active region layer structure, waveguide design, and fabrication parameters) is important for capturing realistic device L–I characteristics, and consequently for predicting the dynamic behavior of the device (see Fig. 3).

III. LASER FEEDBACK INTERFEROMETRY

The mixing of a laser's intracavity EM wave with a reinjected emitted wave after its interaction in the external cavity—frequently
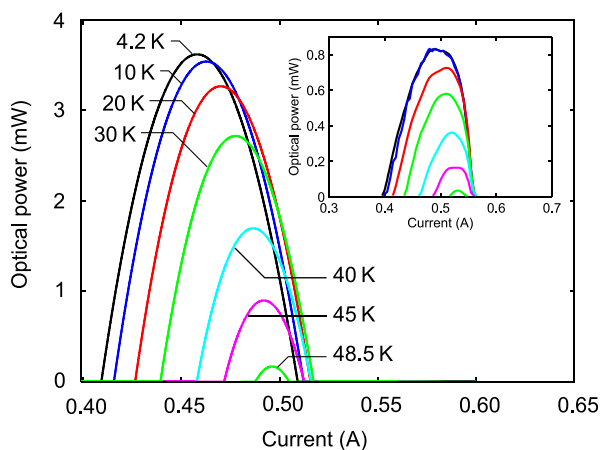
FIG. 3. RRE simulated L–I characteristics of a THz QCL at different operation temperatures. Inset: Measured L–I characteristics at the same temperatures.[18] Reproduced with permission from Agnew et al., Opt. Express **24**, 20554 (2016) Copyright 2016 licensed under a Creative Commons Attribution (CC BY) license.

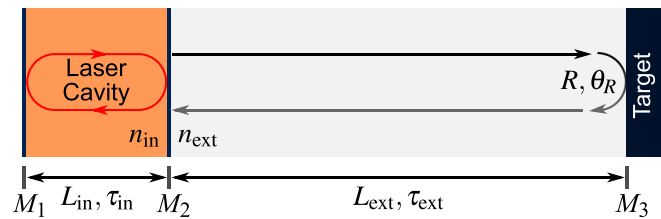**FIG. 4.** Three-mirror model of LFI. The laser is represented as the "internal" cavity with length L_{in}, refractive index n_{in}, and round trip propagation time τ_{in}. Light leaves the internal cavity through the partially transmissive mirror M_2 and traverses the "external" cavity of length L_{ext}, refractive index n_{ext}, and round trip propagation time τ_{ext}. A portion of this light re-enters the laser through M_2 and mixes with the field inside the laser cavity, affecting the operating state of the laser.

referred to as the "SM effect"—is a remarkably universal phenomenon, having been observed in in-plane semiconductor diode lasers, gas lasers, vertical-cavity surface-emitting lasers (VCSELs), fiber and fiber ring lasers, solid-state lasers, microring lasers, quantum dot lasers, interband cascade lasers, and QCLs.

One of the simplest coherent techniques where the emission source can also play the role of a highly-sensitive detector is LFI, and its architecture can be elegantly captured by a three-mirror laser model[56] (see Fig. 4). The reinjected light interferes ("mixes") with the intracavity electric field, causing small variations in the fundamental laser parameters including the threshold gain, emitted power, lasing spectrum, and laser terminal voltage.[57–59] In this model, only one round trip in the external cavity is considered. The phase shift in the external cavity is composed of the transmission phase shift arising from the optical path length as well as the phase change on reflection from the target. The homodyne (coherent) nature of an LFI scheme inherently provides very high sensitivity detection, potentially at the quantum noise limit, and therefore a high signal-to-noise (SNR) ratio can be expected in the SM signal.

While optical feedback affects almost all laser parameters, the two that are most conveniently monitored are the emitted optical power and the voltage across the laser terminals. Of these, monitoring the laser terminal voltage is preferred at THz frequencies as it removes the need for an external detector.[60] The small voltage variation (referred to as the "SM signal") depends on both the amplitude and the phase of the electric field of the reflected laser beam. This configuration thus creates a compact, coherent sensor that can probe information about the laser–target system; see Sec. IV for an overview of applications.

There are five qualitatively different feedback regimes, depending on the strength with which the reinjected wave couples with the laser's internal cavity.[61,62]

I.   Weak optical feedback, for which a broadening or narrowing of the emission line, depending on the phase of the feedback, is observed.
II.   Moderate optical feedback, for which an apparent splitting of the emission line due to rapid mode hopping is observed, remaining dependent on the phase of the feedback.
III. Strong optical feedback, characterized by a return to single frequency emission and a narrowing of the emission line, remaining dependent on the phase of the feedback.
IV.   Coherence collapse, characterized by chaotic dynamics with islands of stability and a broadening of the emission line, remaining only partially dependent on the phase of the feedback.

V.   External cavity mode, characterized by a return to stability, under which the laser–target system effectively operates as an optically pumped (long) EC laser, and is independent of the phase of the feedback.

Regimes I–III, where the operation of the laser under feedback remains dependent on the phase of feedback, by their very nature are those which LFI is concerned with.

The first chart of these five feedback regimes was created by Tkach and Chraplyvy in Ref. 61 for a 1.55-µm DFB interband laser, and reported that the same effects, essentially at the same levels, were observed for FP and cleaved-coupled-cavity (C^3) lasers. This diagram has since been further studied by Donati and Horng, but taken as a representative of the behavior of semiconductor lasers in general.[62] However, Jumpertz et al. in Ref. 63 created the chart for a 5.6 µm DFB MIR QCL, demonstrating that the picture for QCLs is qualitatively different.

In particular, it appears as though QCLs are less susceptible to feedback than interband lasers, resulting in an increased range of stability in the presence of optical feedback,[63] an observation reported by others in the literature.[64,65] Moreover, while there was a distinct regime IV observed in Ref. 63, the authors were unable to observe clear line broadening, and noted with caution that the general absence of relaxation oscillations in QCLs means that, if indeed this regime is coherence collapse, it is not caused by the same route to chaos as for diode lasers (i.e., undamped relaxation oscillations). In any case, the regime IV observed in Ref. 63 appears to be narrower than typically observed in interband lasers, which is in line with Ref. 64 who observed no coherence collapse in both MIR and THz QCLs as well as Ref. 65 who did not observe line broadening. Indeed, Ref. 64 demonstrated that both MIR and THz QCLs can tolerate feedback levels almost two orders of magnitude larger than the equivalent level which would cause instability in a diode laser.

Within feedback regimes suited to LFI, the effects of feedback in any laser which are exploited for sensing are the directly observable fluctuations in the device's optical output power and its terminal voltage. These are equivalent, though theoretically out of phase (for a collimated beam, if the beam is focused, one can observe any phase relation).[66] For conventional laser diodes in the visible and NIR, one usually measures the changes induced by optical feedback in the device's optical output power by means of a photodiode, as it affords superior SNR over monitoring its terminal voltage.[66,67]

However, for LFI with QCLs, there continues to be a preference for voltage sensing. There are two main reasons for this. Firstly, the magnitude of feedback-induced fluctuations is larger than in diode lasers, meaning that adequate signal levels can be obtained by voltage sensing. Secondly, external detectors (particularly at THz frequencies) are typically bulky and require cooling (in the case of sensitive bolometric detectors), or tend to have slow response times (in the case of room-temperature pyroelectric detectors and Golay cells). This slow response severely limits the bandwidth of the sensor when compared to using the laser itself as a receiver.[15,60]

Other effects of feedback can be measured using LFI, from intrinsic device characteristics such as the LEF, phase-noise, or emission spectra, to target characteristics such as changes in the distance or refractive index for the purposes of imaging. The study of EC and coupled cavity (CC) QCLs, though not LFI in the conventional sense, employs much of the same simple resonator analysis.

One can incorporate the dynamic effects of optical feedback by augmenting RRE models for a single longitudinal mode with a photon and a phase equation[18–20] along the lines of the LK formalism.[16] This is particularly well illustrated in Fig. 5, which shows the creation of SM signals via frequency sweeping on short time scales, incorporating both adiabatic and thermal effects. It is, however, relatively straightforward to show that the simple two-level RRE model under optical feedback in the steady state (i.e., in quasi-static operation) further reduces to the excess phase equation, discussed further in Sec. III A below, which is the operational model for LFI. It is rather remarkable that the same model arises seemingly regardless of the laser structure.

A. Model: Excess phase equation

The fundamental equation in LFI is the "excess phase equation" for solution in φ_{FB}

$$\varphi_{FB} - \varphi_s + C \sin(\varphi_{FB} + \arctan \alpha) = 0. \quad (1)$$

Here, C is Acket's characteristic parameter[68,69]

$$C \stackrel{\text{def}}{=} \kappa \frac{\tau_{ext}}{\tau_{in}} \sqrt{1 + \alpha^2}, \quad (2)$$

where α is Henry's LEF,[70] τ_{in} and τ_{ext} denote the round trip time in the laser cavity and the external cavity, respectively, and the coupling strength κ is related to the reflectivities of the emitting facet R_2, the external mirror R, and the reinjection loss factor ε via

$$\kappa \stackrel{\text{def}}{=} \varepsilon \frac{(1 - R_2)}{\sqrt{R_2}} \sqrt{R}. \quad (3)$$

The phase terms appearing in (1) are related to the angular frequency of the solitary laser (i.e., without feedback) ω_s and under feedback ω, as well as the external cavity round trip time τ_{ext} via $\varphi_s \stackrel{\text{def}}{=} \omega_s \tau_{ext}$, $\varphi_{FB} \stackrel{\text{def}}{=} \omega \tau_{ext}$.

It is useful to think of the term φ_s as a "phase stimulus"—symbolically corresponding to the phase accumulated on transmission through the external cavity if the laser was not experiencing optical feedback—and φ_{FB} as a "phase response," corresponding to the actual phase accumulated on transmission through the external cavity. The feedback parameter C dictates the degree of nonlinear coupling between phase stimulus and response, while the LEF α governs the asymmetry of the phase transfer function induced by (1).

Equation (1) can be obtained by considering only the geometry of the optical system of the laser feedback interferometer (i.e., three-mirror model, see Fig. 4). Alternatively, it also arises from the LK model, as well as the two-level RRE model under optical feedback, as its steady state solution.[71]

Note that (1) is a transcendental equation with a unique solution when $C \leq 1$ (weak feedback) and with multiple solutions when $C > 1$ (moderate or strong feedback). Due to the alternating stability of solutions when $C > 1$, physical solutions φ_{FB} to (1) exhibit path dependence (hysteresis) as φ_s, C, or α varies. This characteristic necessitates that some care be taken in solving (1).[72]

The variables C and φ_s as in (1) may be modulated to produce a time-varying SM signal. Changes in the effective optical length of the external cavity result in changes in the phase stimulus φ_s. These can occur due to changes in the laser frequency,[65,73] external cavity's length,[14] or refractive index,[73–75] or in the phase-shift on reflection at the target.[76] Changes in reflection from the target as well as in the external cavity round trip time result in changes in the feedback parameter C. Thus, an SM signal can be created through (i) changing C and fixed φ_s
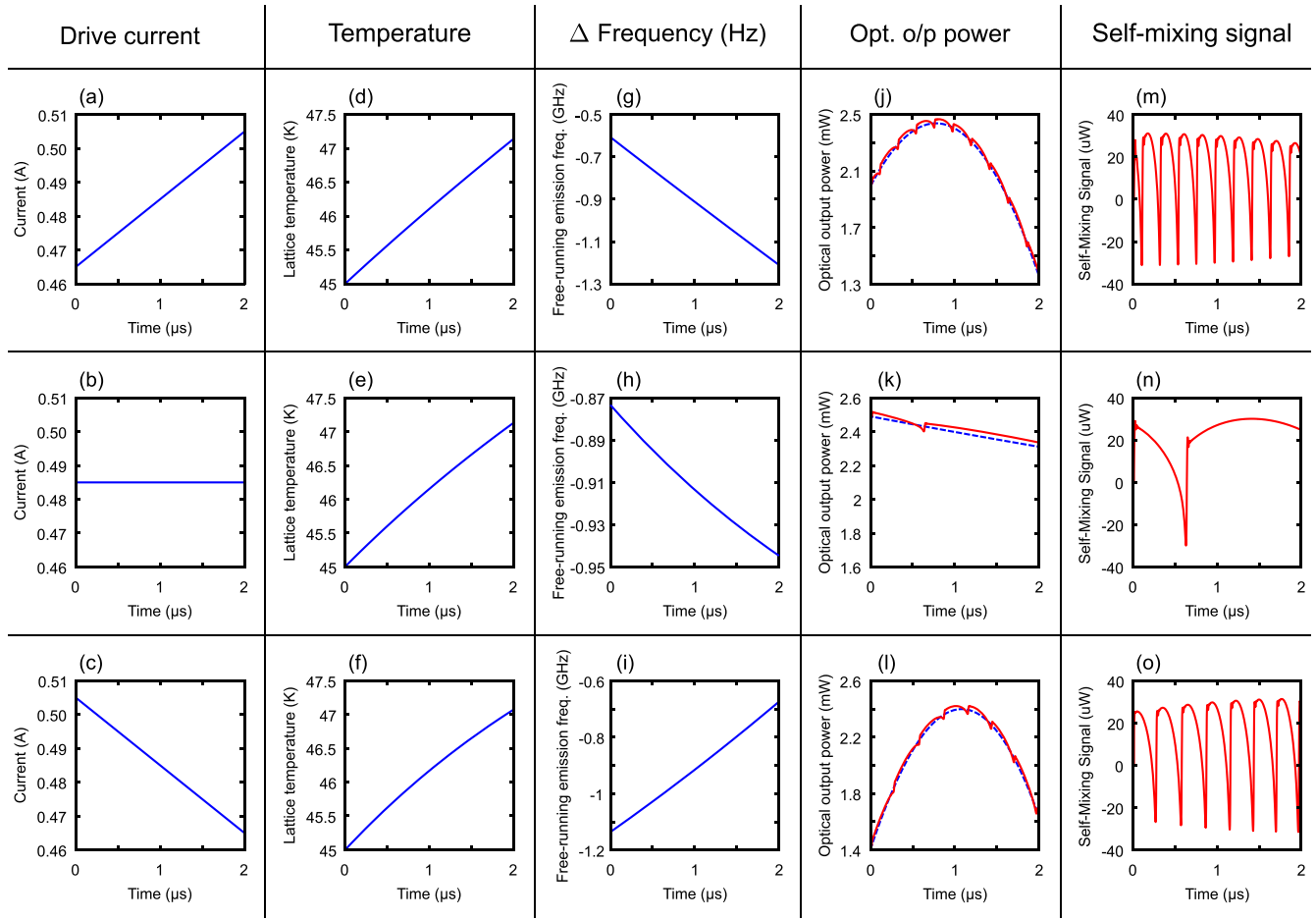
Drive current	Temperature	Δ Frequency (Hz)	Opt. o/p power	Self-mixing signal

FIG. 5. Creation of SM signals on short time scales via frequency sweeping due to adiabatic and thermal effects.[20] Reproduced with permission from Agnew *et al.*, IEEE J. Quantum Electron. **54**, 2300108 (2018). Copyright 2018 IEEE. Top row: Positive current sweep; Middle row: Constant current; Bottom row: Negative current sweep.

(for example, through only change in reflectivity at the external target); (ii) changing φ_s and fixed C (for example, through a change in the laser's emission frequency over a narrow range); or (iii) changing both φ_s and C (for example, by changing the dielectric properties of the target).

The SM signal embedded in the modulated voltage signal (resulting from change in gain due to feedback) is related to the phase change through

$$\Delta V \propto \cos(\varphi_{FB}), \quad (4)$$

where ΔV is the change in the voltage waveform due to optical feedback, and is a function of time through its dependence on the interferometric phase φ_{FB} and the feedback parameter C. The relationship between the phase stimulus, the feedback parameter, and the resulting SM signal (ΔV) is illustrated in Fig. 6.

IV. APPLICATIONS

We will consider two very different uses of the LFI technique: (i) characterization of the very laser experiencing the feedback and (ii) conventional sensing applications. We will address the laser characterization techniques first.

A. Measurement of laser properties under feedback

1. Linewidth and linewidth enhancement factor (α) measurement

The effects of optical feedback on the laser linewidth have long been studied,[70,77,78] with the particular linewidth and value for Henry's LEF α under feedback often depending not only on the level of optical feedback but also on the laser's biasing condition.[79] For a particular optical system, LFI can be used to determine α and linewidth in a number of ways.[80] For QCLs, there are two classes of techniques that have been used to date to experimentally determine α: The simple morphological methods of Yu *et al.*[81] (used for QCLs in Refs. 82–85) and the parameter fitting methods used in Refs. 86 and 87. We briefly describe the first class of methods.

It is straightforward to determine using the excess phase equation (1) that the SM signal $\cos(\varphi_{FB})$ has minima and maxima at

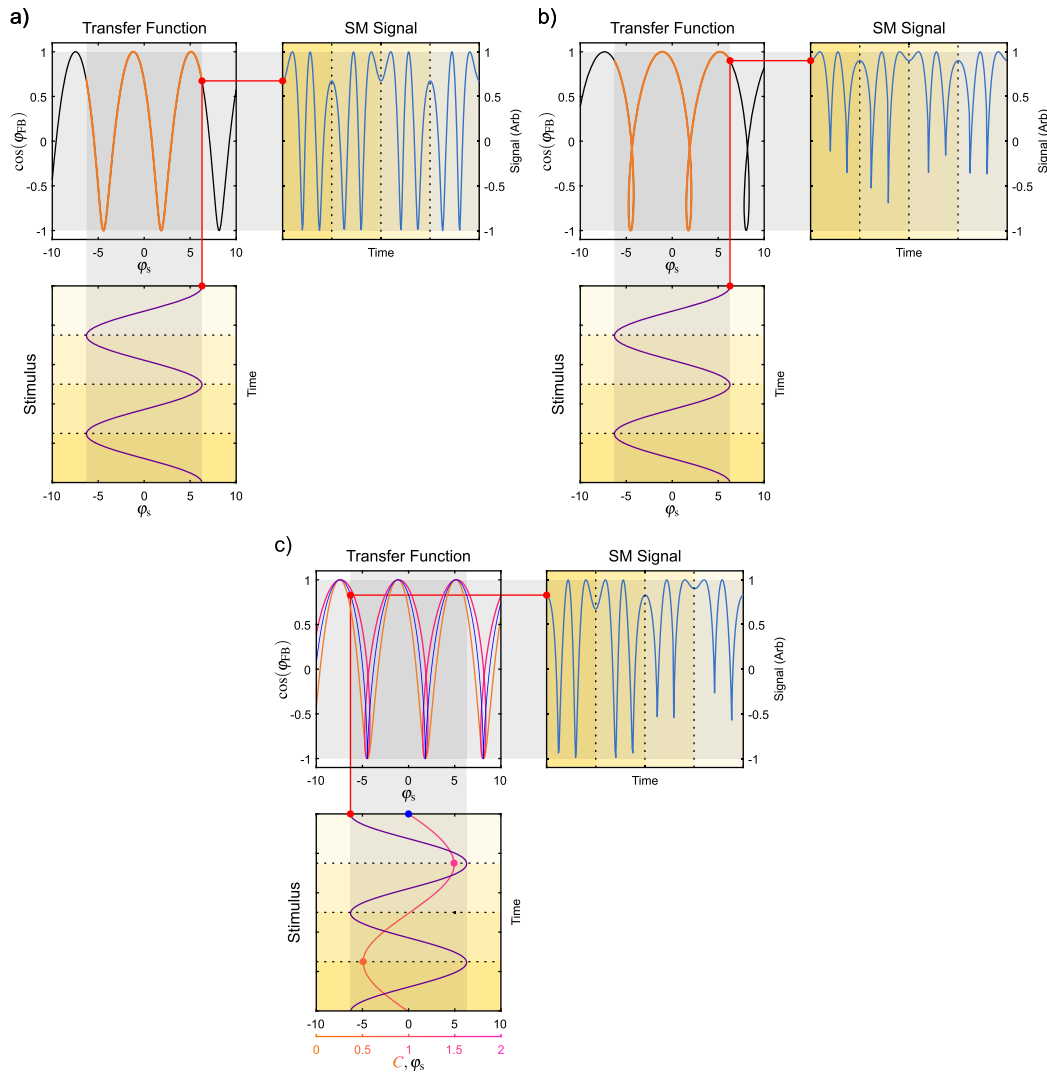$$\varphi_s = m\pi + (-1)^m \frac{C\alpha}{\sqrt{1+\alpha^2}}, \quad m \in \mathbb{Z},$$

FIG. 6. LFI phase-stimulus–signal response transfer function for $\alpha = 0.1$. (a) A sinusoidal phase stimulus for $C = 0.5$. (b) A sinusoidal phase stimulus for $C = 1.5$. (c) A sinusoidal phase stimulus and a sinusoidal feedback parameter stimulus varying periodically between $0.5 \leq C \leq 1.5$. In this case, the transfer function itself varies periodically with C.

with minima corresponding to odd m and maxima corresponding to even m, and has zero-crossings at

$$\varphi_s = (1 + 2m)\frac{\pi}{2} + (-1)^m \frac{C}{\sqrt{1 + \alpha^2}}, \quad m \in \mathbb{Z}.$$

From these, one readily computes the phase-distance from a maximizer to the successive minimizer as

$$A = \pi - 2\frac{C\alpha}{\sqrt{1 + \alpha^2}},$$

and the phase-distance from a zero-crossing between a maximizer and a minimizer to the successive zero-crossing as

$$B = \pi + 2\frac{C}{\sqrt{1 + \alpha^2}}.$$

Relative to the natural period 2π, one obtains the dimensionless quantities

$$\widetilde{A} = \frac{A}{2\pi}, \quad \widetilde{B} = \frac{B}{2\pi},$$

yielding a ready estimate for the linewidth enhancement factor as

$$\frac{0.5 - \widetilde{A}}{\widetilde{B} - 0.5}.$$

The quantities $\widetilde{A}$ and $\widetilde{B}$ can be experimentally determined from an SM signal simply by examining an oscilloscope trace to record (i) the natural period T between successive peaks in the observed signal; (ii) the distance a between a peak and the subsequent trough; and (iii) the distance b between a zero-crossing between a peak and the subsequent trough and the next zero-crossing. Then, α may be estimated as

$$\widehat{\alpha} = \frac{0.5 - a/T}{b/T - 0.5}.$$

This is the approach reported in Ref. 81 and typically used when $C < 1$ (weak feedback). Indeed, the same approach is used in Ref. 82, but with the "first" zero-crossing chosen between a minimizer and a maximizer rather than between a maximizer and a minimizer—leading to the estimate given above being multiplied by a factor of -1. The same experimentally-measured quantities a, b, and T can be used to simultaneously obtain an estimate for C via

$$\widehat{C} = \pi \left(\frac{b}{T} - 0.5 \right) \sqrt{1 + \left(\frac{0.5 - (a/T)}{(b/T) - 0.5} \right)^2}.$$

A similar analysis may be carried out in the case of "moderate feedback" (that is, $1 < C < 4.6$) by considering values of the phase stimulus which correspond to abscissae in the SM signal (rather than maxima and minima, which will not always be achieved due to the path-dependent nature of the solution). In this scenario, due to the path-dependent nature of the solution, care must be taken to distinguish between two situations of increasing and decreasing phase-stimulus. See Ref. 81 for further details.

To experimentally determine the linewidth, Cardilli et al.[88] used the method of Giuliani and Norgia,[89] which employs the linear relationship between phase noise and linewidth to estimate the laser linewidth under optical feedback.

2. Spectrum measurement

Most conventional LFI applications are designed to interrogate an external target or, more generally, the environment external to the laser. In these situations, the SM signal primarily contains information related to such external phenomena. The usual assumption is that the laser is operating in a single mode.

However, provided the characteristics of the external target and the temporal stimulus (for example, motion of a mirror used as an external target) are known, the spectrum of the laser can be inferred from the SM signal. This process is conceptually similar to conventional Fourier transform infrared (FTIR) spectroscopy. As we have demonstrated in Ref. 90, this architecture offers a detector- and alignment-free spectrum analyzer with spectral resolution which compares favorably with the conventional design.

The LFI spectrum analyzer configuration consists of a collimated beam reflected from an external mirror. The external mirror is then longitudinally displaced, and the resulting SM voltage signal is Fourier transformed. The total displacement of the external mirror dictates the resolution of the spectrum analyzer.

In Ref. 90, a cavity extension of 200 mm was used, resulting in a spectral resolution of 750 MHz. However, as noted therein, LFI with THz QCLs has been demonstrated over external path-lengths of greater than 10 m, suggesting that the spectral resolution could in principle be improved to less than 15 MHz. We note here that the spectral resolution demonstrated by this system is insufficient to resolve the laser's intrinsic linewidth.

One key consideration is to ensure that the interferometer operates in the weak feedback regime—that is, with $C < 1$. In practice, this may be achieved by using an attenuator in the external cavity. In this regime, the SM signal (ac component of the linearized terminal voltage signal) can be approximated as a linear combination of SM signals, with each arising from individual longitudinal modes of the solitary laser.[90] The perturbation to the solitary laser frequency due to the SM effect for weak feedback and long external cavity lengths is small—in Ref. 90, being less than the spectral resolution of 750 MHz for the cavity extension of 200 mm. This frequency perturbation for the dominant mode for different levels of feedback was determined by fitting to the excess phase equation, and ranged from just above 125 MHz down to just below 20 MHz.

With $C > 1$, the nonlinear nature of SM gives rise to harmonics in the spectrum of the SM signal, which are an artefact of the LFI detection process and may be misinterpreted as spectral features.

Figure 7 is reproduced from Ref. 90 and shows the emission spectra obtained using the LFI spectrum analyzer as well as conventional FTIR spectroscopy for a range of dc driving currents covering single- and multimode operations of a THz QCL.

3. Phase-noise measurements

In Sec. IV A 2, a scheme to measure the spectra as well as the change in the emission frequency of a single longitudinal mode for QCLs under feedback was discussed. A study of Cardilli and coworkers[88] demonstrated a technique for estimating the RMS phase noise in QCLs from the associated LFI spectrum.

In that study, an MIR QCL emitting on a single longitudinal mode at 6.2 μm just above the threshold current was collimated to an external target. The external target was sinusoidally displaced at a series of target distances [see Fig. 8(a)]. The beam was attenuated to ensure the interferometer was operating with moderate feedback—ensuring the presence of interferometric fringes in the SM signal [see Fig. 8(b)].

At each of these distances, fluctuations of the fast switching time—corresponding to interferometric phase noise, and caused primarily by fluctuations in the laser's frequency—were determined by repeatedly measuring the time of a particular fringe within a single
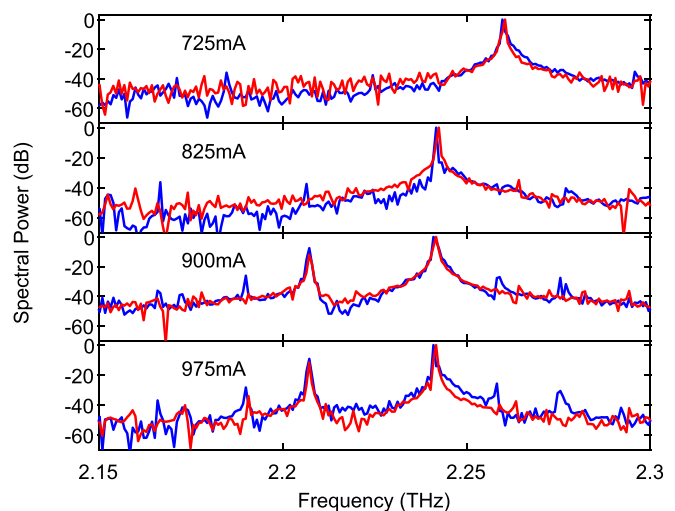

FIG. 7. Emission spectra of a THz QCL in a range of dc driving currents, measured using LFI (blue traces) as well as FTIR spectroscopy (red traces).[90] Reproduced with permission from Keeley et al., Sci. Rep. 7, 7236 (2017). Copyright 2017 licensed under a Creative Commons Attribution (CC BY) license.
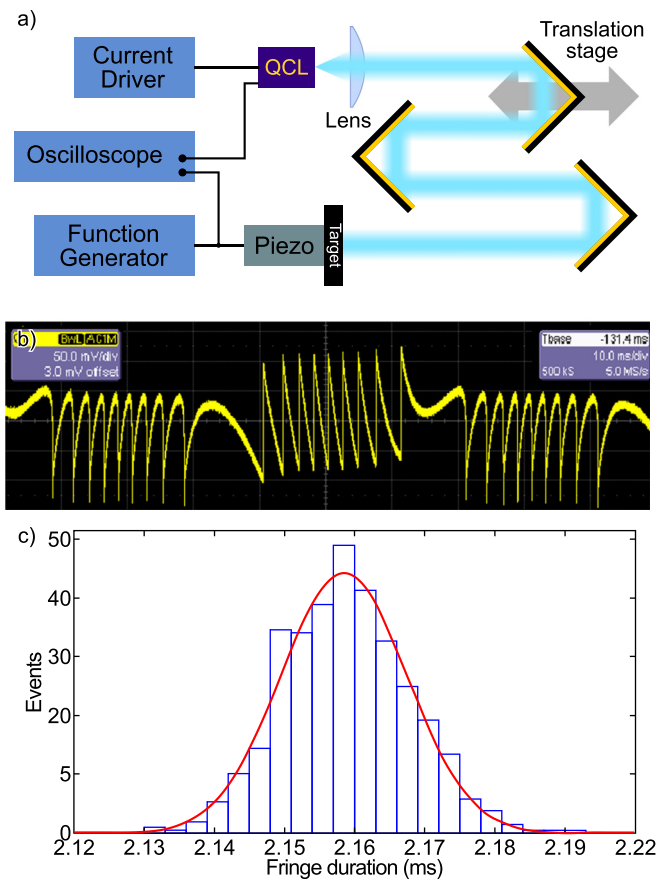
FIG. 8. (a) Schematic of the experimental setup for phase-noise measurements using LFI. (b) Typical SM signal measurements resulting from harmonic displacement of the translation stage in (a). (c) Histogram of the fringe temporal position over a series of repeated displacements, together with a Gaussian fit.[88] Adapted with permission from Appl. Phys. Lett. **108**(3), 031105 (2016). Copyright 2016 AIP Publishing.

repetition of the periodic SM signal, and subsequently fitting a Gaussian to this set of measurements [see Fig. 8(c)].

By assuming that the laser frequency and the target distance are uncorrelated variables, the root mean square (RMS) phase noise $\sqrt{\langle \Delta \varphi^2 \rangle}$ can be decomposed as

$$\sqrt{\langle \Delta \varphi^2 \rangle} = \frac{4\pi}{c} \sqrt{\nu_0^2 \langle \Delta L^2 \rangle + L_0^2 \langle \Delta \nu^2 \rangle},$$

where c is the speed of light in a vacuum, ν is the laser frequency, ν_0 indicates the mean laser frequency, L_0 indicates the external cavity length, $\langle \Delta L^2 \rangle$ represents the mechanical noise in the system, and $\langle \Delta \nu^2 \rangle$ is the linewidth.

By using this equation and the RMS phase noise measurements for a series of external cavity lengths, the linewidth with driving current $I = 1.02 I_{th} = 500$ mA was estimated at 0.28 ± 0.06 MHz and the one with driving current $I = 1.1 I_{th} = 540$ mA was estimated at 0.28 ± 0.08 MHz. We remark here that these measurements are representative of the practical—and not the intrinsic—linewidth of the QCL.

Sections IV A 1–IV A 3 demonstrated that many important spectral characteristics of a semiconductor laser can be obtained from a set of simple LFI experiments. While the methods are general, the application in the THz spectral range is particularly attractive.

B. Sensing applications

1. Imaging

Imaging applications are one of the most exploited applications of LFI with QCLs, holding huge potential in terms of developing stand-off imaging systems, confocal microscopy applications, and biomedical imaging systems. An SM signal can be created by a change in the amplitude of the retroinjected field, or a change in its phase. However, a combination of concurrent changes in both will also lead to the formation of the SM signal. We report here on a number of imaging techniques relying on coherent or incoherent feedback effects. Change in the strength of reflectivity and change in the phase are two techniques that have been exploited for image formation.

The first THz images created using LFI was reported in 2011 by Dean et al.,[60] whereby the temporal change in the SM signal was created through the use of an optical chopper [see Fig. 9(a)].

The modulation employed there changes only the amplitude of the retroinjected field. However, examination of the figures reported therein reveals well-defined interference fringes, resulting from the varying distance between the laser and the target across the image. Indeed, a nontrivial extension of the technique which affords separation of phase and amplitude information was reported in 2013 by Ravaro et al.[93] The early result of Dean et al. (viz., Ref. 60) suggested that the coherent nature of the scheme could be exploited to create three-dimensional images. This study also reported that the strength of the SM signal was two orders of magnitude larger than that usually observed in diode lasers (millivolts as opposed to microvolts). Finally, the region just beyond the lasing threshold was identified as the one with the highest sensitivity to optical feedback in these lasers. We note that the same effect can be achieved by pulsing the laser using a simple square-wave electrical modulation scheme for imaging with LFI. Distinct advantages of such a scheme include: (i) the straightforward creation of the modulating signal, even for high-current lasers and (ii) its natural suitability for lock-in detection.[94]

The study of Mezzapesa et al.[74] makes explicit use of both the amplitude and phase modulation of the SM signal in a very similar configuration to that reported in Ref. 60. Indeed, the potential for separating phase and amplitude information was suggested in those studies.[74] Moreover, concurrent information about amplitude and phase enables the formation of three-dimensional images, and an algorithm for three-dimensional image reconstruction and experimentation has been reported in Ref. 95. The three-dimensional reconstruction was enabled by combining lateral scanning with longitudinal displacement. Therein, an increase in the length of the external cavity changes the phase accumulated in the external cavity, which in turn modulates the SM signal, leading to ability to determine distance change. Alternatively, the effect of longitudinal displacement can be conveniently replaced by sweeping the frequency of the laser.[96]

When forming an image, it is important to keep in mind that the change in phase brought about by longitudinal displacement of a target with a constant complex reflection coefficient (for example, probing two points of a homogeneous material with varying surface

Dia = 25.9 mm   Dia = 16.5 mm   Dia = 19.41 mm   Dia = 24.25 mm

a)   b)   c)   d)

FIG. 9. (a) Image of the obverse of a British two-pence coin, obtained via voltage sensing with LFI using a 2.6 THz QCL, where the beam was modulated by an optical chopper.[60] Reproduced with permission from Dean *et al.*, Opt. Lett. **36**(13), 2587–2589 (2011). Copyright 2011 OSA Publishing. (b) Image of the reverse of a Lunar Year of the Horse 2014 Gold Coin, obtained via voltage sensing with LFI using a 2.9 THz QCL operating in the pulsed mode.[91] Adapted with permission from Appl. Phys. Lett. **107**(1), 011107 (2015). Copyright 2015 AIP Publishing. (c) Amplitude image of the obverse of an Australian five cent coin obtained via swept-frequency LFI using a 2.59 THz QCL. (d) Amplitude contrast image of the reverse of a German 50 cent coin, imaged over 4 s using a scanning mirror, obtained via voltage sensing with LFI using a 3.3 THz QCL, with triangular current modulation.[92] Adapted with permission from Appl. Phys. Lett. **109**(1), 011102 (2016). Copyright 2016 AIP Publishing.

profile) could equally come about as a change in the complex reflection coefficient without any longitudinal displacement (for example, probing two points of a flat target consisting of varying materials). The majority of published works do not explicitly comment on this point. In order to separate the two effects, that is, to enable three-dimensional surface profiling and simultaneous mapping of lateral changes in the refractive index, one must be able to apportion the observed change in phase (modulation of the SM signal) to one or the other cause. Naturally, if one knows that the target is of a homogeneous material, or if the target has a known surface profile (for example, is optically flat), then doing so is straightforward. However, if one cannot make such assumptions, then the two causes can in principle be separated by registering an array of SM signals for a series of longitudinal displacements, and for each a swept-frequency response.

Instead of using a change in voltage across the laser terminals, one can monitor the voltage signal across a quantum cascade (QC) amplifier, integrated with the QCL.[91] In this case, change in the optical feedback can be used to initiate lasing action in the amplifier section, which in turn reduces the voltage across the device terminals. Unlike previous studies, where the QCL was operating in the cw regime, the QC amplifier was pulsed (pulse duration, 3–6 μs) enabling a fast acquisition rate [see Fig. 9(b) for a high-resolution image obtained using this approach].

The swept-frequency LFI technique introduced in Rakić *et al.*[73] and used for materials analysis can also be used simply to create amplitude and phase images [see Fig. 9(c) for an exemplar amplitude image obtained this way]. A study from Wienold *et al.*[92] achieves real-time THz imaging with an impressive framerate of 2 Hz for images of 4.4 K pixels by combining an innovative mechanical scanning scheme with the same swept-frequency technique [see Fig. 9(d) for an image obtained using this approach acquired at 0.25 Hz].

The relatively long wavelength of THz and MIR QCLs imposes a diffraction limit on spatial imaging resolution.[97] A significant increase in spatial resolution can be achieved by using synthetic aperture radar (SAR) techniques, well known in the microwave field,[98,99] or, alternatively, by the use of scanning near-field microscopy techniques.[100–102]

The use of SAR and inverse SAR (ISAR) imaging allows the creation of images with improved spatial resolution by considering the measured signals to be the coherent sum of scattered signals reflected from the target. Multiple measured signals across a synthetic aperture permits one to reconstruct scatterers at the target by synthetic back-propagation to the target surface. This approach was demonstrated in 2014 by Lui *et al.*[103] using LFI with a THz QCL on a standard resolution test target and demonstrated spatial resolutions down to 150 μm, with a theoretical resolution limit of 70 μm—below the diffraction-limited spatial resolution of around 200 μm.

The frequency- and angle-dependent characterization of target reflection—radar cross section (RCS) characterization—has long been regarded as a core application of radar measurement, particularly for military and defense-related purposes. However, objects to be characterized are often very large relative to the microwave frequencies typically employed. In 2015, Lui *et al.*[104] demonstrated RCS characterization using LFI at THz frequencies, at which a target of a smaller physical scale can be used instead—rather than characterizing a target of 5 m at 2.6 GHz, one can characterize a target of 5 mm at 2.6 THz.

In most of these examples, the change in the phase and amplitude jointly works to form an image. The relative strength of each effect can vary from target to target, and from sensing scheme to sensing scheme. The techniques of target pullback (that is, longitudinal displacement) together with frequency sweeping can in principle enable the separation of the two.

a. Displacement and velocity sensing. Displacement and velocity measurement applications are mainstays for sensing techniques, including for LFI where there have been numerous demonstrations at different wavelengths, using different lasers, for different applications.[58,105] When considering the fact that QCLs operate in the MIR or at THz frequencies, one might question the wisdom of employing longer-wavelength lasers when one could employ a shorter wavelength infrared or visible laser. However, several applications that benefit from these wavelengths have been explored.

Detecting movement behind an optically opaque screen (transparent in THz or MIR) comes immediately to mind. Lim *et al.* demonstrated displacement measurement with LFI in a THz QCL,[14] further showing the potential of the technique for detecting movement behind visibly opaque screens which are transparent at THz frequencies.

The technique also allows for concurrent displacement measurement of two targets, located in sequence in the optical path, the first of which is semitransparent.[106] This concurrent monitoring of two SM signals permits for a range of additional applications, stemming from the long wavelength and phase stability of QCLs.[107] If one of the two surfaces is used as a reference, the resolution of the displacement detected at the target interface can be on the order of $\lambda/100$.[108]

An embodiment of this technique for real-time detection of laser ablation was proposed, whereby the depth of the laser-drilled bore is measured using the front surface of the material being machined as a reference.[109] This approach can be augmented by simultaneous measurement of the ablation rate.[110]

When a target is displaced periodically, Valavanis[15] proposes two simple but effective ways of determining the maximum velocity and the amplitude of the displacement. The frequency of the SM signal is related to the maximum velocity of the target and the amplitude of displacement to the change of maximum velocity with respect to frequency.

Displacement measurement when combined with raster-scanning can be used to create three-dimensional profiles of surfaces. Two techniques have been proposed to achieve this—one involving mechanical movement of the target along the laser beam axis[95] or an equivalent frequency modulation of the laser.[96] In the latter case, a depth resolution of better than 100 nm was demonstrated using a QCL emitting at 2.6 THz.

b. Biomedical imaging. Imaging tissues using THz waves has been a mainstay of the scientific literature due to the well-known sensitivity of THz interactions with materials to the water content and changes in the molecular structure. Typically, such biological imaging is carried out using time-domain spectroscopy (TDS).[111–114] It was demonstrated that the swept-frequency LFI can be used as an alternative for imaging tissue samples, permitting the registration of both amplitude- and phase-like images.[115] This scheme operates naturally in the reflection mode, which opens a natural pathway to *in vivo* measurement. However, operation in the transmission mode is possible—for instance, for use on microtomed samples.[115]

The results on the Cdk4 R24C/R24C:Tyr-NRAS Q 61K murine model in Ref. 116—seeking to image malignant melanoma precursor lesions—suggest that LFI can be used to detect early stages of melanoma. Figure 10(a) shows a photograph of a 6 mm murine biopsy in which no lesion is apparent, while Fig. 10(b) shows a SOX10 stained cross section of the same sample, clearly showing a region of healthy

FIG. 10. (a) Photograph of murine model biopsy; (b) En face section of the corresponding SOX10 stained histology; and (c) LFI image.[116] Adapted with permission from Rakić *et al.*, Proc. SPIE 10030 (2016). Copyright 2016 SPIE.[116]

tissues as well as a region containing a lesion. Fig. 10(c) shows an LFI image of the same sample, in which the lesion is clearly visible.

c. Near field imaging. As noted in Sec. IV B 1, there has long been particular interest in biomedical imaging applications in the MIR and THz regions. However, at these frequencies, diffraction effects place a limit on the spatial resolution achievable with far-field techniques. As wavelengths range from ∼3 to 10 μm for MIR and ∼50 to 300 μm for THz, this precludes the direct imaging of features on the cellular scale (below 10 μm)—for applications such as intercellular imaging and intracellular chemical mapping.[117] The probing of solid-state materials on these scales in the MIR and THz range is another key driver for imaging below the diffraction limits,[118] with potential applications including the mapping of charge carriers in semiconductors and nanostructures,[119] the microscopic investigation of quantum dots and nanowires,[120,121] and investigation of metamaterials.[122]

Consequently, recent years have seen increased interest in near-field imaging with THz and MIR waves due to the capacity of near-field techniques to resolve spatial features well beyond the diffraction limit, and at the same time probe the response of materials at THz frequencies and in the MIR.[100,101,119–122]

One predominant approach to near-field imaging in the MIR and THz regions is to use scattering-type near-field optical microscopy (s-SNOM). In s-SNOM, an atomic force microscope (AFM) drives a sharp metallic tip in the tapping mode or intermittent contact mode to scan the sample. An external light source is coupled to the apex of the tip and scattered light is collected. Crucially, due to the near-field interaction between the excited tip and the sample surface, the enhanced scattered signal is sensitive to the local (near-field) dielectric properties of the sample.

In 2008, the first QCL-based s-SNOM was reported using an external detector by Huber *et al.*[119] Arguably, the simplest solution to s-SNOM at THz frequencies and in the MIR is to combine the laser and the detector in one device and to use an LFI detection scheme. Craig *et al.* performed MIR near-field spectroscopy of trace explosives using such an approach, achieving a spectral resolution of 0.25 cm^{-1} and a spatial resolution of 25 nm with an EC QCL source tunable from 7.1 to 7.9 μm.[123] This is particularly relevant in the THz range due to the lack of fast and sensitive detectors. A 2016 study by Dean and co-workers demonstrates this approach,[124] achieving a spatial resolution of $\lambda/100$ using a 2.53 THz QCL. Subsequently, in 2017, Degl'Innocenti *et al.* augmented the system with a custom-designed tuning fork to enhance the sensitivity of the detection scheme[102] and Giordano *et al.* demonstrated such a system combined with an AFM with improved image quality[125] (see Fig. 11).

2. Refractive index measurement

An interesting application of LFI lies in materials analysis and extraction of a complex refractive index of a remote target with the aid of calibration standards.[69,73] In principle, the SM signal is imprinted with information on the target's reflectivity and phase-shift on reflection. With a suitably designed experiment, their relative impact can be measured; with calibration standards, it is possible to estimate their numerical value. However, different signal processing and parameter extraction methods are required depending on the nature of the target.
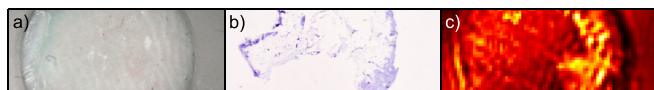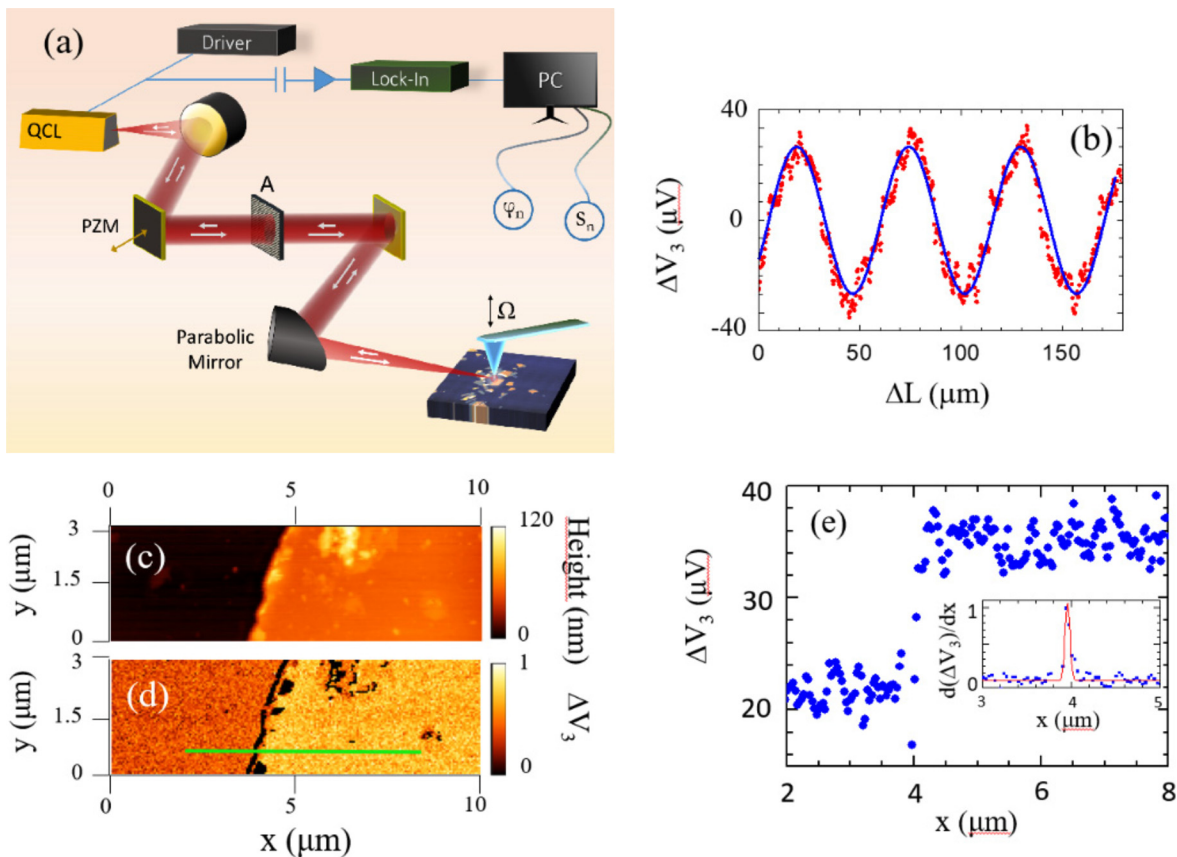
FIG. 11. LFI scattering type near field optical microscope with nanometer resolution at THz frequencies.[125] Reprinted with permission from Giordano et al., Opt. Express **26**(14), 18423–18435 (2018). Copyright 2018 OSA Publishing. (a) Schematic of the experimental setup; (b) 3rd harmonic component of the SM signal; (c) the AFM topographic image of gold on a silicon sample; (d) the corresponding LFI image; and (e) the depth profile with reference to the green line in (d).

The case that is closest to the theoretical ideal is the extraction of optical constants of polished homogeneous and isotropic samples.[69,73] The main difficulty here lies in differentiating between a change in phase due to a change in the phase-shift on reflection and a change in phase otherwise accumulated in the external cavity (for example, resulting from a change in the target distance). More challenging is the case of granular materials (such as plastic explosives).[126] Their random nature presents one with additional complexity requiring methods which rely on ensemble characteristics rather than the characteristics of a single point on the target. Finally, the small change in the refractive index brought about by free-carrier injection can also be identified,[127] opening up the possibility for application in the semiconductor industry including the dopant profile and level measurements.

a. Homogeneous materials analysis. The shape of an SM waveform is fundamentally affected by the reflectivity of the external target through the feedback parameter C [see (2)]—it is proportional to the amplitude reflection coefficient, among other factors [see (3)].

An SM waveform is also affected by the external target's phase-shift on reflection, although it is difficult—but not impossible—to tease apart from the transmission phase in the case where the external target is homogeneous, isotropic, optically flat, and well-aligned. When the

current of the laser is linearly modulated, the second order effect is a linear chirp of the lasing frequency. This chirp leads to a predictable linear dependence of the transmission phase over time. The phase-stimulus in this situation can be ideally written as

$$\varphi(t) = \varphi_0 + \frac{\Phi_\Delta}{T} t - \theta_R,$$

where θ_R is the phase-shift on reflection, φ_0 is the round trip phase-shift on transmission at the beginning of the frequency sweep, T is the period of the linear current (frequency) sweep, and Φ_Δ is the linearized change in phase caused by the current sweep.

This swept-frequency LFI experiment can be used with calibration standards to extract the complex refractive index of such a target.[73,128] For a detailed description of the method and the relationship between the complex refractive index of a target and accuracy of the extracted refractive index, see Ref. 69. Similarly, Bertling and co-authors demonstrated the use of swept-frequency LFI to estimate the ethanol content of alcoholic solutions.[75]

b. Granular materials analysis. The technique outlined in Sec. IV B 2 can in principle be used for materials analysis of a single point on an external target. However, it requires sample preparation that

can be challenging or unrealistic for certain types of targets. An application of particular interest that has shown promise in the far infrared (FIR) and THz is materials analysis of plastic explosives (see Fig. 12).

However, there is additional complexity associated with extracting the complex refractive index of such a granular material embedded in an inert matrix.[126] The idea presented therein relies on the same swept-frequency approach—the key difference is that the material of interest is interrogated multiple times over different spatial locations, leading to a collection of SM signals, each imprinted with slightly different complex refractive indices. The approach taken in Ref. 126 is to set up an over-determined linear system of equations with parameters $C/\sqrt{1+\alpha^2}$, $C\alpha/\sqrt{1+\alpha^2}$, and $\theta_R - \varphi_0$. Solving this system of equations via least squares over a series of spatial patches on the target results in a "cloud" of points in parameter space (see Fig. 12).

The potential phase ambiguity in $\theta_R - \varphi_0$ is resolved automatically by unwrapping the phase across two periods and employing the well-known K-means algorithm and the Silhouette Coefficient (see Ref. 126 for details). A central point in parameter space is then selected using the mean-shift algorithm, and is taken as representative of the ensemble characteristics of the target. This can then be used with calibration standards to obtain numerical estimates of the effective optical characteristics of the granular material.

This noncontact procedure could potentially be carried out with pulsed QCLs[18] (enabling higher-temperature operation), or extended heterogeneous laser structures with a wider tuning range.[19]

c. Free carrier distribution. Mezzapesa and coworkers reported in Ref. 127 the imaging of the distribution of the free carrier concentration and the corresponding spatial variation of the refractive index via LFI using a THz QCL, enjoying the usual benefits of coherent sensing without the need for an additional detector (see Fig. 13).

This photoinduced change in the spatial refractive index can also be used for beam formation and beam manipulation, as reported in
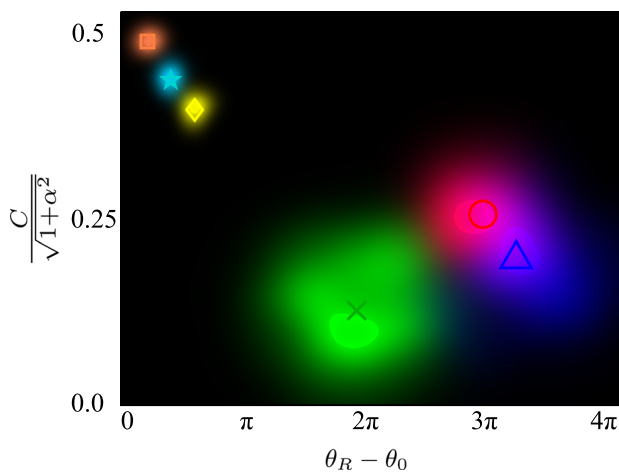

FIG. 12. The distribution of the point cloud together with the centroid for three plastic explosives: METABEL, SEMTEX, SX2 (indicated by red, green, and blue clouds and circle, cross, and triangle markers, respectively). Also shown for comparison are the point clouds for three homogeneous plastics HDPE, PC, and HDPE Black (indicated by orange, cyan, and yellow clouds and square, star, and diamond markers, respectively).[126] Reproduced with permission from Han *et al.*, Sensors **16**, 352, 2016. Copyright 2016 licensed under a Creative Commons Attribution (CC BY) license.
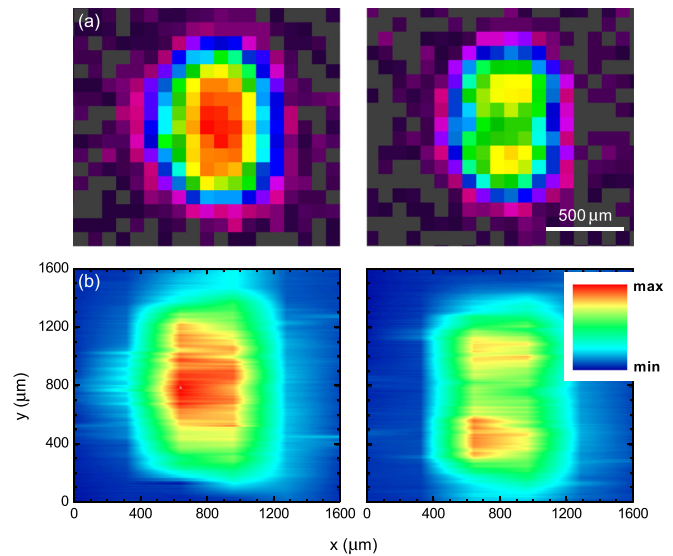

FIG. 13. (a) Representative intensity distributions of the infrared pump laser by placing a charge-coupled device (CCD) camera at the sample position. The pattern was computer controlled by a spatial light modulator (SLM) and projected onto the silicon surface. Dark pixels of the SLM liquid crystal maintain the polarization of the incident light and define the exposed area. (b) Terahertz imaging in the reflection mode of a photoexcited electron plasma on semiconductors. The spatial distribution of free carrier charges corresponds to the structured beam profile.[127] Reproduced with permission from Appl. Phys. Lett. **104**(4), 041112 (2014). Copyright 2014 AIP Publishing.

Ref. 76. In that work, photoinduced metamaterials were created through the manipulation of the photocarrier distribution on a semiconductor wafer by means of a NIR cw optical pump beam through a spatial light modulator (SLM). A periodic spatial pattern on the wafer that is of subwavelength results in significant anisotropy in the resulting material, giving rise to the possibility of simultaneous positive and negative permittivities of a beam's polarization states. This approach has only optical components and avoids the need for fabrication, pointing toward unprecedented control of the emission characteristics of THz QCLs.

3. Gas detection

A major area of application of LFI with QCLs is to trace gas detection,[129–133] although it appears in the literature under the moniker of optical-feedback cavity-enhanced absorption spectroscopy (OF-CEAS). The combination of QCLs with LFI has been demonstrated for sensing traces of formaldehyde,[134] atmospheric methane,[135,136] the hydroperoxyl radical in a plasma jet,[137] water vapor measurements,[138,139] and for multiple trace gasses,[140] to highlight only a few. In the THz frequency range, the narrow linewidths offered by QCLs is also particularly well-suited to high-resolution spectroscopy of gases, for which absorption features are typically spectrally narrow.[141–146]

The theoretical formalism appears a little different from LFI at first sight (see, e.g., Ref. 147, Sec. 5.3.1)—however, the basic model in OF-CEAS is the three-mirror model and gives rise to the excess phase equation given in (1) for which the simple model of a
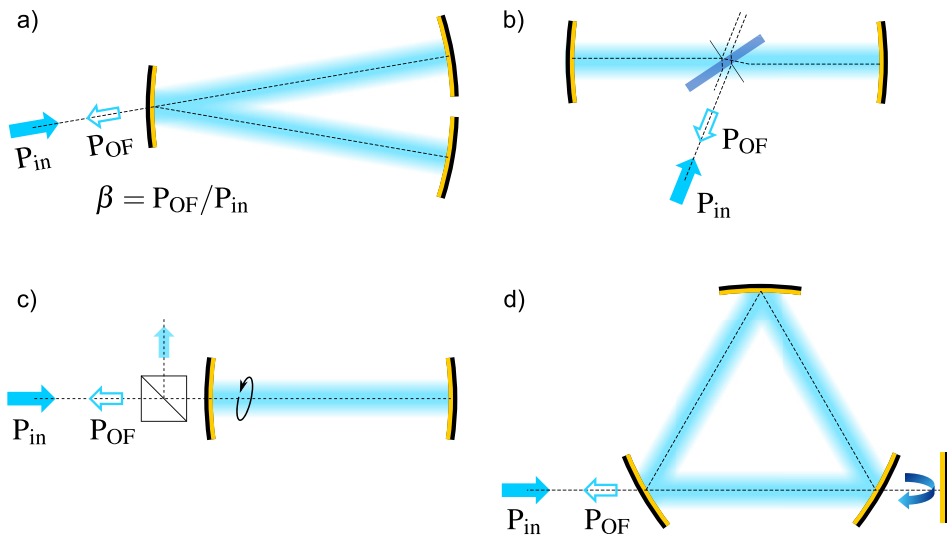
FIG. 14. Schematic drawing of four different cavity geometries for OF-CEAS.[147] From Morville, *Cavity-Enhanced Spectroscopy and Sensing*. Copyright 2014 Springer. Adapted by permission from Springer Nature Customer Service Center GmbH. (a) V-shaped cavity. (b) Brewster angle cavity. (c) Linear cavity with residual mirror birefringence. (d) Ring cavity.

frequency-independent external target reflectivity—arising in (1)–(3)—is replaced by a general reflection transfer function.

If one denotes by $h(\omega)$ the field transfer function, then the frequency-dependent feedback level [c.f. (2)] is

$$C(\omega) := \kappa(\omega) \, \frac{\tau_{\text{ext}}}{\tau_{\text{in}}} \, \sqrt{1 + \alpha^2},$$

where the frequency-dependent coupling strength [c.f. (3)] is given by

$$\kappa(\omega) := \varepsilon \, \frac{(1 - R_2)}{\sqrt{R_2}} \, |h(\omega)|.$$

The corresponding version of the excess phase equation [c.f. (1)] reads as

$$\varphi_{\text{FB}} - \varphi_s + C(\omega) \sin \left(\varphi_{\text{FB}} + \arctan(\alpha) - \text{Arg}(h(\omega)) \right) = 0,$$

where $\text{Arg}(\cdot)$ denotes the principal value of the argument of a complex number, taken here to lie in the interval $(-\pi, \pi]$.

The change in laser gain is modeled as

$$\Delta g \propto \cos \left(\varphi_{\text{FB}} - \text{Arg}(h(\omega)) \right).$$

For small perturbations under which the gain can be locally linearized, the model given above leads to a SM power or voltage signal of the same functional form [c.f. (4)]. Note that when $h(\omega) = \sqrt{R_{\text{ext}}}$ is the real amplitude reflection coefficient of the external target, then these equations reduce to the basic LFI model given in Sec. III A.

The idea in OF-CEAS is to self-lock the laser to an external optical cavity containing the sample under study. The effect of the external cavity is to spectrally filter the emitted beam and the optical feedback induces laser linewidth narrowing to lower than the spectral width of the cavity modes.[148] By sweeping the laser's frequency, the frequency-dependent effect of transmission through the external cavity directly impacts the SM signal through $|h(\omega)|$. This can be measured by monitoring the laser's terminal voltage or optical output power.

The precise nature of the field transfer function depends on the configuration of the OF-CEAS instrument.[147,149,150] Figure 14 shows a few common cavity geometries.

A particularly striking illustration of the effect of $|h(\omega)|$ on the SM signal is shown in Fig. 15.

V. STATE OF THE ART AND THE ROAD AHEAD

The pairing of QCL devices as high-power coherent sources of MIR and THz radiation with the high-sensitivity and optically simple technique of LFI has distinct advantages, particularly in the THz region where there is presently a lack of convenient alternatives for high-speed high-sensitivity detection. Applications demonstrated to date range from measuring internal laser characteristics such as
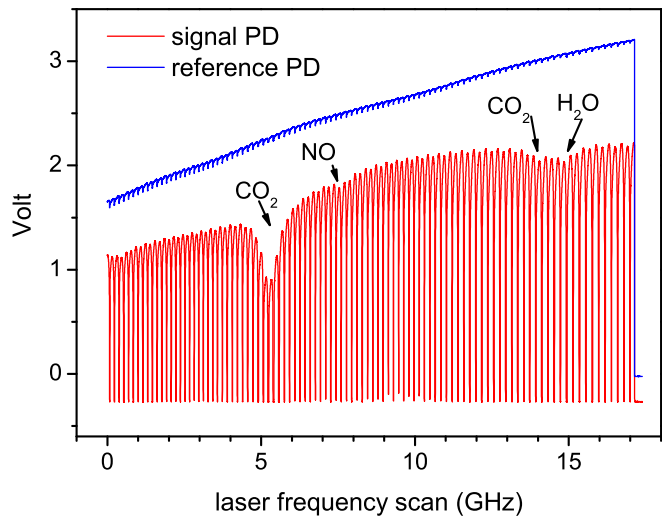

FIG. 15. Signal from the light transmitted through an OF-CEAS V-shaped cavity geometry as the laser frequency is the 5.26 μm MIR QCL which is frequency-swept (red trace).[151] The cavity is filled with ambient air at 100 mbar. Absorption lines of NO, CO_2, and H_2O are observed. Adapted by permission from Ventrillard *et al.*, Appl. Phys. B **123**, 180 (2017). Copyright 2017 Springer Nature Customer Service Center GmbH.

emission spectra, linewidth, and phase noise to trace gas detection, materials analysis, biomedical imaging, and near-field imaging.

In the majority of these applications, the device is operated in cw mode. However, we see a great deal of potential for applications employing pulsed mode operation (especially in the THz range), which results in higher emitted power and higher temperature operation, as well as potential for time-gating. Our modeling work suggests that pulsed time of flight as well as more sophisticated swept frequency LFI radar schemes are feasible. Accurate modeling of the dynamic behavior of QCLs under optical feedback presents the need for device-specific models. Such models are becoming available for THz QCLs that take into account the temperature and current/voltage dependence of laser characteristics.[17,18,21] These models can be used to predict the behavior of pulsed QCLs experiencing optical feedback,[18,20] which was a key step to realizing the most recently demonstrated pulsed LFI system.[152,153]

We also see potential for multispectral measurements using tunable QCLs, particularly in the domain of materials analysis—probing an external target at a plurality of narrow spectral bands could act as a way to nondestructively, spectrally "fingerprint" materials in the reflection mode at a distance.[19]

ACKNOWLEDGMENTS

REFERENCES

[1] J. Faist, F. Capasso, D. L. Sivco, C. Sirtori, A. L. Hutchinson, and A. Y. Cho, "Quantum cascade laser," Science **264**, 553–556 (1994).

[2] Editorial, "Quantum cascade celebration," Nat. Photonics **8**, 577 (2014).

[3] M. S. Vitiello, G. Scalari, B. Williams, and P. De Natale, "Quantum cascade lasers: 20 years of challenges," Opt. Express **23**, 5167–5182 (2015).

[4] R. Köhler, A. Tredicucci, F. Beltram, H. E. Beere, E. H. Linfield, A. G. Davies, D. A. Ritchie, R. C. Iotti, and F. Rossi, "Terahertz semiconductor-heterostructure laser," Nature **417**, 156–159 (2002).

[5] S. S. Dhillon, M. S. Vitiello, E. H. Linfield, A. G. Davies, M. C. Hoffmann, J. Booske, C. Paoloni, M. Gensch, P. Weightman, G. P. Williams, E. Castro-Camus, D. R. S. Cumming, F. Simoens, I. Escorcia-Carranza, J. Grant, S. Lucyszyn, M. Kuwata-Gonokami, K. Konishi, M. Koch, C. A. Schmuttenmaer, T. L. Cocker, R. Huber, A. G. Markelz, Z. D. Taylor, V. P. Wallace, J. A. Zeitler, J. Sibik, T. M. Korter, B. Ellison, S. Rea, P. Goldsmith, K. B. Cooper, R. Appleby, D. Pardo, P. G. Huggard, V. Krozer, H. Shams, M. Fice, C. Renaud, A. Seeds, A. Stöhr, M. Naftaly, N. Ridler, R. Clarke, J. E. Cunningham, and M. B. Johnston, "The 2017 terahertz science and technology roadmap," J. Phys. D: Appl. Phys. **50**, 043001 (2017).

[6] D. M. Mittleman, "Twenty years of terahertz imaging," Opt. Express **26**, 9417–9431 (2018).

[7] H. Guerboukha, K. Nallappan, and M. Skorobogatiy, "Toward real-time terahertz imaging," Adv. Opt. Photonics **10**, 843–938 (2018).

[8] S. Donati, "Responsivity and noise of self-mixing photodetection schemes," IEEE J. Quantum. Electron. **47**, 1428–1433 (2011).

[9] A. J. Seeds, M. J. Fice, K. Balakier, M. Natrella, O. Mitrofanov, M. Lamponi, M. Chtioui, F. van Dijk, M. Pepper, G. Aeppli, A. G. Davies, P. Dean, E. H. Linfield, and C. C. Renaud, "Coherent terahertz photonics," Opt. Express **21**, 22988–23000 (2013).

[10] S. Bartalini, M. Vitiello, and P. De Natale, "Quantum cascade lasers: A versatile source for precise measurements in the mid/far-infrared range," Meas. Sci. Technol. **25**, 12001–12017 (2014).

[11] P. Dean, A. Valavanis, J. Keeley, K. Bertling, Y. Lim, R. Alhathlool, A. Burnett, L. Li, S. Khanna, D. Indjin, T. Taimre, A. D. Rakić, E. H. Linfield, and A. G. Davies, "Terahertz imaging using quantum cascade lasers—a review of systems and applications," J. Phys. D: Appl. Phys. **47**, 374008 (2014).

[12] E. Hack and P. Zolliker, "Terahertz holography for imaging amplitude and phase objects," Opt. Express **22**, 16079–16086 (2014).

[13] M. Locatelli, M. Ravaro, S. Bartalini, L. Consolino, M. S. Vitiello, R. Cicchi, F. Pavone, and P. De Natale, "Real-time terahertz digital holography with a quantum cascade laser," Sci. Rep. **5**, 13566 (2015).

[14] Y. L. Lim, P. Dean, M. Nikolić, R. Kliese, S. P. Khanna, M. Lachab, A. Valavanis, D. Indjin, Z. Ikonic, P. Harrison, E. H. Linfield, A. G. Davies, S. J. Wilson, and A. D. Rakić, "Demonstration of a self-mixing displacement sensor based on THz quantum cascade lasers," Appl. Phys. Lett. **99**, 081108 (2011).

[15] A. Valavanis, P. Dean, Y. L. Lim, R. Alhathlool, M. Nikolić, R. Kliese, S. P. Khanna, D. Indjin, S. J. Wilson, A. D. Rakić, E. H. Linfield, and A. G. Davies, "Self-mixing interferometry with terahertz quantum cascade lasers," IEEE Sens. J. **13**, 37–43 (2013).

[16] R. Lang and K. Kobayashi, "External optical feedback effects on semiconductor injection laser properties," IEEE J. Quantum Electron. **16**, 347–355 (1980).

[17] G. Agnew, A. Grier, T. Taimre, Y. L. Lim, M. Nikolić, A. Valavanis, J. Cooper, P. Dean, S. P. Khanna, M. Lachab, E. H. Linfield, A. G. Davies, P. Harrison, Z. Ikonić, D. Indjin, and A. D. Rakić, "Efficient prediction of terahertz quantum cascade laser dynamics from steady-state simulations," Appl. Phys. Lett. **106**, 161105 (2015).

[18] G. Agnew, A. Grier, T. Taimre, Y. L. Lim, K. Bertling, Z. Ikonić, A. Valavanis, P. Dean, J. Cooper, S. P. Khanna, M. Lachab, E. H. Linfield, A. G. Davies, P. Harrison, D. Indjin, and A. D. Rakić, "Model for a pulsed terahertz quantum cascade laser under optical feedback," Opt. Express **24**, 20554–20570 (2016).

[19] X. Qi, G. Agnew, I. Kundu, T. Taimre, Y. L. Lim, K. Bertling, P. Dean, A. Grier, A. Valavanis, E. H. Linfield, A. G. Davies, D. Indjin, and A. D. Rakić, "Multi-spectral terahertz sensing: Proposal for a coupled-cavity quantum cascade laser based optical feedback interferometer," Opt. Express **25**, 10153–10165 (2017).

[20] G. Agnew, A. Grier, T. Taimre, K. Bertling, Y. L. Lim, Z. Ikonic, P. Dean, A. Valavanis, D. Indjin, and A. D. Rakic, "Frequency tuning range control in pulsed terahertz quantum-cascade lasers: Applications in interferometry," IEEE J. Quantum Electron. **54**, 2300108 (2018).

[21] A. Grier, P. Dean, A. Valavanis, J. Keeley, I. Kundu, J. D. Cooper, G. Agnew, T. Taimre, Y. L. Lim, K. Bertling, A. D. Rakic, L. H. Li, P. Harrison, E. H. Linfield, Z. Ikonić, A. G. Davies, and D. Indjin, "Origin of terminal voltage variations due to self-mixing in terahertz frequency quantum cascade lasers," Opt. Express **24**, 21948–21956 (2016).

[22] C. Gmachl, F. Capasso, D. L. Sivco, and A. Y. Cho, "Recent progress in quantum cascade lasers and applications," Rep. Prog. Phys. **64**, 1533 (2001).

[23] G. Scalari, C. Walther, M. Fischer, R. Terazzi, H. Beere, D. Ritchie, and J. Faist, "THz and sub-THz quantum cascade lasers," Laser Photonics Rev. **3**, 45–66 (2009).

[24] G. Liang, T. Liu, and Q. J. Wang, "Recent developments of terahertz quantum cascade lasers," IEEE J. Sel. Top. Quantum Electron. **23**, 1200118 (2017).

[25] G. Purvis, "MWIR centre field in R&D," III-Vs Rev. **19**, 20–25 (2006).

[26] L. Esaki and R. Tsu, "Superlattice and negative differential conductivity in semiconductors," IBM J. Res. Dev. **14**, 61–65 (1970).

[27] R. F. Kazarinov and R. A. Suris, "Possibility of the amplification of electromagnetic waves in a semiconductor with a superlattice," Sov. Phys. Semicond. **5**, 707 (1971).

[28] For example, the GaAs/AlGaAs heterostructure system has two Reststrahlen bands, GaAs-like and AlAs-like appearing within ∼ 260–400 cm^{-1}; [Ref. 154, Chap. 2] equivalently ∼25–38.5 µm, ∼32.2–49.6 meV, or ∼7.78–12 THz., [AlAs-like: ∼350–400 cm^{-1}, ∼25–28.5 µm, ∼43.5–49.6 meV, or 10.5–12 THz. GaAs-like: ∼260–300 cm^{-1}, ∼25–33.3 µm, ∼32.2–37.2 meV, or ∼7.78–9 THz.] Rule-of-thumb values for "the Reststrahlen band" of ∼25–60 µm or ∼5–12 THz appear to be in frequent use within the QCL literature. However, it should not be concluded that QCLs cannot be designed to

operate in this range, simply that any particular semiconductor system has its limitations. Indeed, there have been recent reports of InGaAs/GaAsSb QCL operating at 28.3 μm, within the AlAs-like Reststrahlen band, with suggestions of suitable semiconductor material systems to span the entire range.[155,156]

[29]M. A. Belkin and F. Capasso, "New frontiers in quantum cascade lasers: High performance room temperature terahertz sources," Phys. Scr. **90**, 118002 (2015).

[30]S. Bartalini, S. Borri, P. Cancio, A. Castrillo, I. Galli, G. Giusfredi, D. Mazzotti, L. Gianfrani, and P. De Natale, "Observing the intrinsic linewidth of a quantum-cascade laser: Beyond the Schawlow-Townes limit," Phys. Rev. Lett. **104**, 083904 (2010).

[31]S. Bartalini, S. Borri, I. Galli, G. Giusfredi, D. Mazzotti, T. Edamura, N. Akikusa, M. Yamanishi, and P. D. Natale, "Measuring frequency noise and intrinsic linewidth of a room-temperature DFB quantum cascade laser," Opt. Express **19**, 17996–18003 (2011).

[32]L. Tombez, S. Schilt, J. D. Francesco, P. Thomann, and D. Hofstetter, "Temperature dependence of the frequency noise in a mid-IR DFB quantum cascade laser from cryogenic to room temperature," Opt. Express **20**, 6851–6859 (2012).

[33]M. S. Vitiello, L. Consolino, S. Bartalini, A. Taschin, A. Tredicucci, M. Inguscio, and P. De Natale, "Quantum-limited frequency fluctuations in a terahertz laser," Nat. Photonics **6**, 525–528 (2012).

[34]L. Consolino, S. Jung, A. Campa, M. De Regis, S. Pal, J. H. Kim, K. Fujita, A. Ito, M. Hitaka, S. Bartalini, P. De Natale, M. A. Belkin, and M. S. Vitiello, "Spectral purity and tunability of terahertz quantum cascade laser sources based on intra-cavity difference-frequency generation," Sci. Adv. **3**, e1603317 (2017).

[35]D. Indjin, P. Harrison, R. W. Kelsall, and Z. Ikonić, "Mechanisms of temperature performance degradation in terahertz quantum-cascade lasers," Appl. Phys. Lett. **82**, 1347–1349 (2003).

[36]B. A. Burnett and B. S. Williams, "Origins of terahertz difference frequency susceptibility in midinfrared quantum cascade lasers," Phys. Rev. Appl. **5**, 034013 (2016).

[37]J. Faist, *Quantum Cascade Lasers* (Oxford University Press, Oxford, 2013).

[38]K. Fujita, S. Jung, Y. Jiang, J. H. Kim, A. Nakanishi, A. Ito, M. Hitaka, T. Edamura, and M. A. Belkin, "Recent progress in terahertz difference-frequency quantum cascade laser sources," Nanophotonics **7**, 1795–1817 (2018).

[39]M. Beck, D. Hofstetter, T. Aellen, J. Faist, U. Oesterle, M. Ilegems, E. Gini, and H. Melchior, "Continuous wave operation of a mid-infrared semiconductor laser at room temperature," Science **295**, 301–305 (2002).

[40]L. H. Li, L. Chen, J. R. Freeman, M. Salih, P. Dean, A. G. Davies, and E. H. Linfield, "Multi-watt high-power THz frequency quantum cascade lasers," Electron. Lett. **53**, 799–800 (2017).

[41]B. S. Williams, S. Kumar, Q. Hu, and J. L. Reno, "High-power terahertz quantum-cascade lasers," Electron. Lett. **42**, 89–91 (2006).

[42]C. Jirauschek and T. Kubis, "Modeling techniques for quantum cascade lasers," Appl. Phys. Rev. **1**, 011307 (2014).

[43]A. Demić, A. Grier, Z. Ikonić, A. Valavanis, C. A. Evans, R. Mohandas, L. Li, E. H. Linfield, A. G. Davies, and D. Indjin, "Infinite-period density-matrix model for terahertz-frequency quantum cascade lasers," IEEE Trans. THz Sci. Technol. **7**, 368–377 (2017).

[44]A. Grier, "Modelling the optical and electronic transport properties of AlGaAs and AlGaN intersubband devices and optimisation of quantum cascade laser active regions," Ph.D. thesis, The University of Leeds, 2015.

[45]A. Pan, B. A. Burnett, C. O. Chui, and B. S. Williams, "Density matrix modeling of quantum cascade lasers without an artificially localized basis: A generalized scattering approach," Phys. Rev. B **96**, 085308 (2017).

[46]I. Savić, N. Vukmirović, Z. Ikonić, D. Indjin, R. W. Kelsall, P. Harrison, and V. Milanović, "Density matrix theory of transport and gain in quantum cascade lasers in a magnetic field," Phys. Rev. B **76**, 165310 (2007).

[47]A. Wacker, M. Lindskog, and D. O. Winge, "Nonequilibrium Green's function model for simulation of quantum cascade laser devices under operating conditions," IEEE J. Sel. Top. Quantum Electron. **19**, 1–11 (2013).

[48]D. O. Winge, M. Franckié, and A. Wacker, "Simulating terahertz quantum cascade lasers: Trends from samples from different labs," J. Appl. Phys. **120**, 114302 (2016).

[49]N. Vukmirović, Z. Ikonić, D. Indjin, and P. Harrison, "Quantum transport in semiconductor quantum dot superlattices: Electron–phonon resonances and polaron effects," Phys. Rev. B **76**, 245313 (2007).

[50]R. Köhler, R. C. Iotti, A. Tredicucci, and F. Rossi, "Design and simulation of terahertz quantum cascade lasers," Appl. Phys. Lett. **79**, 3920–3922 (2001).

[51]H. Li, J. C. Cao, and J. T. Lü, "Monte Carlo simulation of carrier transport and output characteristics of terahertz quantum cascade lasers," J. Appl. Phys. **103**, 103113 (2008).

[52]R. C. Iotti and F. Rossi, "Nature of charge transport in quantum-cascade lasers," Phys. Rev. Lett. **87**, 146603 (2001).

[53]P. Borowik, J.-L. Thobel, and L. Adamowicz, "Monte Carlo modeling applied to studies of quantum cascade lasers," Opt. Quantum Electron. **49**, 96 (2017).

[54]A. Hamadou, S. Lamari, and J.-L. Thobel, "Dynamic modeling of a midinfrared quantum cascade laser," J. Appl. Phys. **105**, 093116 (2009).

[55]Y. Petitjean, F. Destic, J. C. Mollier, and C. Sirtori, "Dynamic modeling of terahertz quantum cascade lasers," IEEE J. Sel. Top. Quantum Electron. **17**, 22–29 (2011).

[56]K. Petermann, *Laser Diode Modulation and Noise* (Kluwer Academic Publishers, Dordrecht, 1991).

[57]S. Donati, "Developing self-mixing interferometry for instrumentation and measurements," Laser Photonics Rev. **6**, 393–417 (2012).

[58]G. Giuliani, M. Norgia, S. Donati, and T. Bosch, "Laser diode self-mixing technique for sensing applications," J. Opt. A: Pure Appl. Opt. **4**, S283–S294 (2002).

[59]G. Giuliani and S. Donati, "Laser interferometry," in *Unlocking Dynamical Diversity: Optical Feedback Effects on Semiconductor Lasers*, edited by D. M. Kane and K. A. Shore (John Wiley & Sons, Chichester, 2005), Chap. 7, pp. 217–255.

[60]P. Dean, Y. L. Lim, A. Valavanis, R. Kliese, M. Nikolić, S. P. Khanna, M. Lachab, D. Indjin, Z. Ikonić, P. Harrison, A. D. Rakić, E. H. Linfield, and A. G. Davis, "Terahertz imaging through self-mixing in a quantum cascade laser," Opt. Lett. **36**, 2587–2589 (2011).

[61]R. W. Tkach and A. R. Chraplyvy, "Regimes of feedback effects in 1.5-μm distributed feedback lasers," J. Lightwave Technol. **4**, 1655–1661 (1986).

[62]S. Donati and R.-H. Horng, "The diagram of feedback regimes revisited," IEEE J. Sel. Top. Quantum Electron. **19**, 1500309 (2013).

[63]L. Jumpertz, M. Carras, K. Schires, and F. Grillot, "Regimes of external optical feedback in 5.6 μm distributed feedback mid-infrared quantum cascade lasers," Appl. Phys. Lett. **105**, 131112 (2014).

[64]F. Mezzapesa, L. Columbo, M. Brambilla, M. Dabbicco, S. Borri, M. Vitiello, H. Beere, D. Ritchie, and G. Scamarcio, "Intrinsic stability of quantum cascade lasers against optical feedback," Opt. Express **21**, 13748–13757 (2013).

[65]H.-W. Hübers, H. Richter, R. Eichholz, M. Wienold, K. Biermann, L. Schrottke, and H. T. Grahn, "Heterodyne spectroscopy of frequency instabilities in terahertz quantum-cascade lasers induced by optical feedback," IEEE J. Sel. Top. Quantum Electron. **23**, 1800306 (2017).

[66]Y. L. Lim, K. Bertling, P. Rio, J. R. Tucker, and A. D. Rakić, "Displacement and distance measurement using the change in junction voltage across a laser diode due to the self-mixing effect," Proc. SPIE **6038**, 60381O (2005).

[67]J. A. Roumy, J. Perchoux, Y. L. Lim, T. Taimre, A. D. Rakić, and T. Bosch, "Effect of injection current and temperature on signal strength in a laser diode optical feedback interferometer," Appl. Opt. **54**, 312–318 (2015).

[68]G. A. Acket, D. Lenstra, J. den Boef, and B. H. Verbeek, "The influence of feedback intensity on longitudinal mode properties and optical noise in index-guided semiconductor lasers," IEEE J. Quantum Electron. **20**, 1163–1169 (1984).

[69]T. Taimre and A. D. Rakić, "On the nature of Acket's characteristic parameter C in semiconductor lasers," Appl. Opt. **53**, 1001–1006 (2014).

[70]C. H. Henry, "Theory of the linewidth of semiconductor lasers," IEEE J. Quantum Electron. **18**, 259–264 (1982).

[71]T. Taimre, M. Nikolić, K. Bertling, Y. L. Lim, T. Bosch, and A. D. Rakić, "Laser feedback interferometry: A tutorial on the self-mixing effect for coherent sensing," Adv. Opt. Photonics **7**, 570–631 (2015).

[72]R. Kliese, T. Taimre, A. Bakar, Y. L. Lim, K. Bertling, M. Nikolić, J. Perchoux, T. Bosch, and A. D. Rakić, "Solving self-mixing equations for arbitrary feedback levels: A concise algorithm," Appl. Opt. **53**, 3723–3736 (2014).

[73]A. D. Rakić, T. Taimre, K. Bertling, Y. L. Lim, P. Dean, D. Indjin, Z. Ikonić, P. Harrison, A. Valavanis, S. P. Khanna, M. Lachab, S. J. Wilson, E. H. Linfield, and A. G. Davies, "Swept-frequency feedback interferometry using terahertz frequency QCLs: A method for imaging and materials analysis," Opt. Express **21**, 22194–22205 (2013).

[74]F. Mezzapesa, M. Petruzzella, M. Dabbicco, H. Beere, D. Ritchie, M. Vitiello, and G. Scamarcio, "Continuous-wave reflection imaging using optical feedback interferometry in terahertz and mid-infrared quantum cascade lasers," IEEE Trans. Terahertz Sci. Technol. **4**, 631–633 (2014).

[75]K. Bertling, S. Han, T. Wu, C. Zhao, Y. L. Lim, P. Dean, S. P. Khanna, D. Indjin, E. H. Linfield, A. G. Davies, S. J. Wilson, T. Taimre, and A. D. Rakić, "Determining ethanol content of liquid solutions using laser feedback interferometry with a terahertz quantum cascade laser," IEEE Sens. Lett. **2**, 3501604 (2018).

[76]F. P. Mezzapesa, L. L. Columbo, C. Rizza, M. Brambilla, A. Ciattoni, M. Dabbicco, M. S. Vitiello, and G. Scamarcio, "Photo-generated metamaterials induce modulation of cw terahertz quantum cascade lasers," Sci. Rep. **5**, 16207 (2015).

[77]G. P. Agrawal, "Line narrowing in a single-mode injection laser due to external optical feedback," IEEE J. Quantum Electron. **20**, 468–471 (1984).

[78]M. Osiński and J. Buus, "Linewidth broadening factor in semiconductor lasers—an overview," IEEE J. Quantum Electron. **23**, 9–29 (1987).

[79]Y. Yu and J. Xi, "Influence of external optical feedback on the alpha factor of semiconductor lasers," Opt. Lett. **38**, 1781–1783 (2013).

[80]G. Giuliani, S. Donati, and W. Elsäßer, "Measurement of linewidth enhancement factor of different semiconductor lasers in operating conditions," Proc. SPIE **6184**, 61841D (2006).

[81]Y. Yu, G. Giuliani, and S. Donati, "Measurement of the linewidth enhancement factor of semiconductor lasers based on the optical feedback self-mixing effect," IEEE Photonics Technol. Lett. **16**, 990–992 (2004).

[82]J. von Staden, T. Gensty, W. Elsäßer, G. Giuliani, and C. Mann, "Measurements of the α factor of a distributed-feedback quantum cascade laser by an optical feedback self-mixing technique," Opt. Lett. **31**, 2574–2576 (2006).

[83]R. P. Green, J.-H. Xu, L. Mahler, A. Tredicucci, F. Beltram, G. Giuliani, H. E. Beere, and D. A. Ritchie, "Linewidth enhancement factor of terahertz quantum cascade lasers," Appl. Phys. Lett. **92**, 071106 (2008).

[84]M. Ishihara, T. Morimoto, S. Furuta, K. Kasahara, N. Akikusa, K. Fujita, and T. Edamura, "Linewidth enhancement factor of quantum cascade lasers with single phonon resonance-continuum depopulation structure on Peltier cooler," Electron. Lett. **45**, 1168–1169 (2009).

[85]T. Inoue, K. Tsushima, S. Mori, and K. Kasahara, "Quantum cascade laser intensity noise under external feedback conditions estimated from self-mixing method," Electron. Lett. **49**, 407–409 (2013).

[86]N. Kumazaki, Y. Takagi, M. Ishihara, K. Kasahara, A. Sugiyama, N. Akikusa, and T. Edamura, "Detuning characteristics of the linewidth enhancement factor of a midinfrared quantum cascade laser," Appl. Phys. Lett. **92**, 121104 (2008).

[87]N. Kumazaki, Y. Takagi, M. Ishihara, K. Kasahara, A. Sugiyama, N. Akikusa, and T. Edamura, "Spectral behavior of linewidth enhancement factor of a mid-infrared quantum cascade laser," Jpn. J. Appl. Phys. **47**, 6320–6326 (2008).

[88]M. C. Cardilli, M. Dabbicco, F. P. Mezzapesa, and G. Scamarcio, "Linewidth measurement of mid infrared quantum cascade laser by optical feedback interferometry," Appl. Phys. Lett. **108**, 031105 (2016).

[89]G. Giuliani and M. Norgia, "Laser diode linewidth measurement by means of self-mixing interferometry," IEEE Photonics Technol. Lett. **12**, 1028–1030 (2000).

[90]J. Keeley, J. Freeman, K. Bertling, Y. L. Lim, R. A. Mohandas, T. Taimre, L. H. Li, D. Indjin, A. D. Rakić, E. H. Linfield, A. G. Davies, and P. Dean, "Measurement of the emission spectrum of a semiconductor laser using laser-feedback interferometry," Sci. Rep. **7**, 7236 (2017).

[91]Y. Ren, R. Wallis, D. S. Jessop, R. Degl'Innocenti, A. Klimont, H. E. Beere, and D. A. Ritchie, "Fast terahertz imaging using a quantum cascade amplifier," Appl. Phys. Lett. **107**, 011107 (2015).

[92]M. Wienold, T. Hagelschuer, N. Rothbart, L. Schrottke, K. Biermann, H. Grahn, and H.-W. Hübers, "Real-time terahertz imaging through self-mixing in a quantum-cascade laser," Appl. Phys. Lett. **109**, 011102 (2016).

[93]M. Ravaro, V. Jagtap, G. Santarelli, C. Sirtori, L. Li, S. Khanna, E. H. Linfield, and S. Barbieri, "Continuous-wave coherent imaging with terahertz quantum cascade lasers using electro-optic harmonic sampling," Appl. Phys. Lett. **102**, 091107–091107 (2013).

[94]K. Bertling, T. Taimre, G. Agnew, Y. L. Lim, P. Dean, D. Indjin, S. Höfling, R. Weih, M. Kamp, M. von Edlinger, J. Koeth, and A. D. Rakić, "Simple electrical modulation scheme for laser feedback imaging," IEEE Sens. J. **16**, 1937–1942 (2016).

[95]P. Dean, A. Valavanis, J. Keeley, K. Bertling, Y. L. Lim, R. Alhathlool, S. Chowdhury, T. Taimre, L. H. Li, D. Indjin, S. J. Wilson, A. D. Rakić, E. H. Linfield, and A. G. Davies, "Coherent three-dimensional terahertz imaging through self-mixing in a quantum cascade laser," Appl. Phys. Lett. **103**, 181112 (2013).

[96]J. Keeley, P. Dean, A. Valavanis, K. Bertling, Y. L. Lim, R. Alhathlool, T. Taimre, L. H. Li, D. Indjin, A. D. Rakić, E. H. Linfield, and A. G. Davies, "Three-dimensional terahertz imaging using swept-frequency feedback interferometry with a quantum cascade laser," Opt. Lett. **40**, 994–997 (2015).

[97]M. Born and E. Wolf, *Principles of Optics: Electromagnetic Theory of Propagation, Interference and Diffraction of Light*, 6th (corrected) ed. (Pergamon Press, Oxford, 1980).

[98]D. L. Mensa, *High Resolution Radar Cross-Section Imaging* (Artech House, Boston, MA, 1991).

[99]R. J. Sullivan, *Radar Foundations for Imaging and Advanced Concepts* (Scitech, Raleigh, NC, 2004).

[100]A. J. L. Adam, "Review of near-field terahertz measurement methods and their applications," J. Infrared Millimeter Terahertz Waves **32**, 976 (2011).

[101]O. Mitrofanov, L. Viti, E. Dardanis, M. C. Giordano, D. Ercolani, A. Politano, L. Sorba, and M. S. Vitiello, "Near-field terahertz probes with room-temperature nanodetectors for subwavelength resolution imaging," Sci. Rep. **7**, 44240 (2017).

[102]R. Degl'Innocenti, R. Wallis, B. Wei, L. Xiao, S. J. Kindness, O. Mitrofanov, P. Braeuninger-Weimer, S. Hofmann, H. E. Beere, and D. A. Ritchie, "Terahertz nanoscopy of plasmonic resonances with a quantum cascade laser," ACS Photonics **4**, 2150–2157 (2017).

[103]H. Lui, T. Taimre, K. Bertling, Y. Lim, P. Dean, S. Khanna, M. Lachab, A. Valavanis, D. Indjin, E. Linfield, and A. Davies, and A. D. Rakić, "Terahertz inverse synthetic aperture radar imaging using self-mixing interferometry with a quantum cascade laser," Opt. Lett. **39**, 2629–2632 (2014).

[104]H. Lui, T. Taimre, K. Bertling, Y. Lim, P. Dean, S. Khanna, M. Lachab, A. Valavanis, D. Indjin, E. Linfield, A. Davies, and A. D. Rakić, "Terahertz radar cross-section characterisation using laser feedback interferometry with quantum cascade laser," Electron. Lett. **51**, 1774–1776 (2015).

[105]S. Donati, "Laser interferometry by induced modulation of cavity field," J. Appl. Phys. **49**, 495–497 (1978).

[106]G. de Risi, L. L. Columbo, and M. Brambilla, "Study of QCL laser sources for the realization of advanced sensors," Sensors **15**, 19140–19156 (2015).

[107]F. P. Mezzapesa, L. L. Columbo, M. Dabbicco, M. Brambilla, and G. Scamarcio, "QCL-based nonlinear sensing of independent targets dynamics," Opt. Express **22**, 5867–5874 (2014).

[108]F. P. Mezzapesa, L. L. Columbo, G. De Risi, M. Brambilla, M. Dabbicco, V. Spagnolo, and G. Scamarcio, "Nanoscale displacement sensing based on nonlinear frequency mixing in quantum cascade lasers," IEEE J. Sel. Top. Quantum Electron. **21**, 107–114 (2015).

[109]F. P. Mezzapesa, V. Spagnolo, A. Ancona, and G. Scamarcio, "Detection of ultrafast laser ablation using quantum cascade laser-based sensing," Appl. Phys. Lett. **101**, 171107 (2012).

[110]F. P. Mezzapesa, L. L. Columbo, A. Ancona, M. Dabbicco, V. Spagnolo, M. Brambilla, P. M. Lugarà, and G. Scamarcio, "On line sensing of ultrafast laser microdrilling processes by optical feedback interferometry," Phys. Procedia **41**, 670–676 (2013).

[111]E. Pickwell and V. P. Wallace, "Biomedical applications of terahertz technology," J. Phys. D: Appl. Phys. **39**, R301 (2006).

[112]V. P. Wallace, A. J. Fitzgerald, E. Pickwell, R. J. Pye, P. F. Taday, N. Flanagan, and T. Ha, "Terahertz pulsed spectroscopy of human basal cell carcinoma," Appl. Spectrosc. **60**, 1127–1133 (2006).

[113]S. Y. Huang, Y. X. J. Wang, D. K. W. Yeung, A. T. Ahuja, Y.-T. Zhang, and E. Pickwell-MacPherson, "Tissue characterization using terahertz pulsed imaging in reflection geometry," Phys. Med. Biol. **54**, 149 (2009).

[114]C. Yu, S. Fan, Y. Sun, and E. Pickwell-MacPherson, "The potential of terahertz imaging for cancer diagnosis: A review of investigations to date," Quant. Imaging Med. Surg. **2**, 33–45 (2012).

[115]Y. L. Lim, T. Taimre, K. Bertling, P. Dean, D. Indjin, A. Valavanis, S. P. Khanna, M. Lachab, H. Schaider, T. W. Prow, H. P. Soyer, S. J. Wilson, E. H. Linfield, A. G. Davies, and A. D. Rakić, "High-contrast coherent terahertz imaging of porcine tissue via swept-frequency feedback interferometry," Biomed. Opt. Express **5**, 3981–3989 (2014).

[116]A. D. Rakić, Y. L. Lim, T. Taimre, G. Agnew, X. Qi, K. Bertling, S. Han, S. J. Wilson, I. Kundu, A. Grier, Z. Ikonić, A. Valavanis, A. Demić, J. Keeley, L. H. Li, E. H. Linfield, A. G. Davies, P. Harrison, B. Ferguson, G. Walker, T. Prow, D. Indjin, and H. P. Soyer, "Optical feedback effects on terahertz quantum cascade lasers: Modelling and applications," Proc. SPIE **10030**, 16 (2016).

[117]H. Amrania, L. Drummond, R. C. Coombes, S. Shousha, L. Woodley-Barker, K. Weir, W. Hart, I. Carter, and C. C. Phillips, "New IR imaging modalities for cancer detection and for intra-cell chemical mapping with a sub-diffraction mid-ir s-snom," Faraday Discuss. **187**, 539–553 (2016).

[118]H. Wang, L. Wang, and X. G. Xu, "Scattering-type scanning near-field optical microscopy with low-repetition-rate pulsed light source through phase-domain sampling," Nat. Commun. **7**, 13212 (2016).

[119]A. J. Huber, F. Keilmann, J. Wittborn, J. Aizpurua, and R. Hillenbrand, "Terahertz near-field nanoscopy of mobile carriers in single semiconductor nanodevices," Nano Lett. **8**, 3766–3770 (2008).

[120]R. Jacob, S. Winnerl, M. Fehrenbacher, J. Bhattacharyya, H. Schneider, M. T. Wenzel, H.-G. von Ribbeck, L. M. Eng, P. Atkinson, O. G. Schmidt, and M. Helm, "Intersublevel spectroscopy on single inas-quantum dots by terahertz near-field microscopy," Nano Lett. **12**, 4336–4340 (2012).

[121]M. Eisele, T. L. Cocker, M. A. Huber, M. Plankl, L. Viti, D. Ercolani, L. Sorba, M. S. Vitiello, and R. Huber, "Ultrafast multi-terahertz nano-spectroscopy with sub-cycle temporal resolution," Nat. Photonics **8**, 841–845 (2014).

[122]A. Bitzer, H. Merbold, A. Thoman, T. Feurer, H. Helm, and M. Walther, "Terahertz near-field imaging of electric and magnetic resonances of a planar metamaterial," Opt. Express **17**, 3826–3834 (2009).

[123]I. M. Craig, M. S. Taubman, A. S. Lea, M. C. Phillips, E. E. Josberger, and M. B. Raschke, "Infrared near-field spectroscopy of trace explosives using an external cavity quantum cascade laser," Opt. Express **21**, 30401–30414 (2013).

[124]P. Dean, O. Mitrofanov, J. Keeley, I. Kundu, L. Li, E. H. Linfield, and A. Giles Davies, "Apertureless near-field terahertz imaging using the self-mixing effect in a quantum cascade laser," Appl. Phys. Lett. **108**, 091113 (2016).

[125]M. C. Giordano, S. Mastel, C. Liewald, L. L. Columbo, M. Brambilla, L. Viti, A. Politano, K. Zhang, L. Li, A. G. Davies, E. H. Linfield, R. Hillenbrand, F. Keilmann, G. Scamarcio, and M. S. Vitiello, "Phase-resolved terahertz self-detection near-field microscopy," Opt. Express **26**, 18423–18435 (2018).

[126]S. Han, K. Bertling, P. Dean, J. Keeley, A. D. Burnett, Y. L. Lim, S. P. Khanna, A. Valavanis, E. H. Linfield, A. G. Davies, T. Taimre, and A. D. Rakić, "Laser feedback interferometry as a tool for analysis of granular materials at terahertz frequencies: Towards imaging and identification of plastic explosives," Sensors **16**, 352 (2016).

[127]F. Mezzapesa, L. Columbo, M. Brambilla, M. Dabbicco, M. Vitiello, and G. Scamarcio, "Imaging of free carriers in semiconductors via optical feedback in terahertz quantum cascade lasers," Appl. Phys. Lett. **104**, 041112 (2014).

[128]A. Rakić, P. Dean, A. G. Davies, D. Indjin, E. H. Linfield, S. J. Wilson, T. Taimre, K. Bertling, and Y. L. Lim, "A laser system for imaging and materials analysis," Australia patent WO2015024058 A1 (22 August 2014).

[129]G. Maisons, P. Gorrotxategi-Carbajo, M. Carras, and D. Romanini, "Optical-feedback cavity-enhanced absorption spectroscopy with a quantum cascade laser," Opt. Lett. **35**, 3607–3609 (2010).

[130]J. Habig, J. Nadolny, J. Meinen, H. Saathoff, and T. Leisner, "Optical feedback cavity enhanced absorption spectroscopy: Effective adjustment of the feedback-phase," Appl. Phys. B **106**, 491–499 (2012).

[131]M. C. Phillips and M. S. Taubman, "Intracavity sensing via compliance voltage in an external cavity quantum cascade laser," Opt. Lett. **37**, 2664–2666 (2012).

[132]A. G. V. Bergin, G. Hancock, G. A. D. Ritchie, and D. Weidmann, "Linear cavity optical-feedback cavity-enhanced absorption spectroscopy with a quantum cascade laser," Opt. Lett. **38**, 2475–2477 (2013).

[133]K. M. Manfred, K. M. Hunter, L. Ciaffoni, and G. A. Ritchie, "ICL based OF-CEAS: A sensitive tool for analytical chemistry," Anal. Chem. **89**, 902–909 (2017).

[134]P. Gorrotxategi-Carbajo, E. Fasci, I. Ventrillard, M. Carras, G. Maisons, and D. Romanini, "Optical-feedback cavity-enhanced absorption spectroscopy with a quantum-cascade laser yields the lowest formaldehyde detection limit," Appl. Phys. A **110**, 309–314 (2013).

[135]K. M. Manfred, L. Ciaffoni, and G. A. Ritchie, "Optical-feedback cavity-enhanced absorption spectroscopy in a linear cavity: Model and experiments," Appl. Phys. B **120**, 329–339 (2015).

[136]N. Lang, U. Macherius, M. Wiese, H. Zimmermann, J. Röpcke, and J. van Helden, "Sensitive CH_4 detection applying quantum cascade laser based optical feedback cavity-enhanced absorption spectroscopy," Opt. Express **24**, A536–A543 (2016).

[137]M. Gianella, S. Reuter, A. L. Aguila, G. A. Ritchie, and J.-P. H. van Helden, "Detection of HO_2 in an atmospheric pressure plasma jet using optical feedback cavity-enhanced absorption spectroscopy," New J. Phys. **18**, 113027 (2016).

[138]A. Campargue, S. Kassi, D. Mondelain, S. Vasilchenko, and D. Romanini, "Accurate laboratory determination of the near-infrared water vapor self-continuum: A test of the MT_CKD model," J. Geophys. Res. Atmos. **121**, 13,180–13,203, https://doi.org/10.1002/2016JD025531 (2016).

[139]A. Campargue, S. Mikhailenko, S. Vasilchenko, C. Reynaud, S. Béguier, P. Čermák, D. Mondelain, S. Kassi, and D. Romanini, "The absorption spectrum of water vapor in the 2.2 μm transparency window: High sensitivity measurements and spectroscopic database," J. Quantum Spectrosc. Radiat. Transfer **189**, 407–416 (2017).

[140]M. C. Phillips, M. S. Taubman, and J. Kriesel, "Use of external cavity quantum cascade laser compliance voltage in real-time trace gas sensing of multiple chemicals," Proc. SPIE **9370**, 93700Z (2015).

[141]A. Campa, L. Consolino, M. Ravaro, D. Mazzotti, M. S. Vitiello, S. Bartalini, and P. D. Natale, "High-Q resonant cavities for terahertz quantum cascade lasers," Opt. Express **23**, 3751–3761 (2015).

[142]T. Hagelschuer, M. Wienold, H. Richter, L. Schrottke, K. Biermann, H. T. Grahn, and H.-W. Hübers, "Terahertz gas spectroscopy through self-mixing in a quantum-cascade laser," Appl. Phys. Lett. **109**, 191101 (2016).

[143]T. Hagelschuer, M. Wienold, H. Richter, L. Schrottke, H. T. Grahn, and H.-W. Hübers, "Real-time gas sensing based on optical feedback in a terahertz quantum-cascade laser," Opt. Express **25**, 30203–30213 (2017).

[144]R. Chhantyal-Pun, A. Valavanis, J. T. Keeley, P. Rubino, I. Kundu, Y. Han, P. Dean, L. Li, A. G. Davies, and E. H. Linfield, "Gas spectroscopy with integrated frequency monitoring through self-mixing in a terahertz quantum-cascade laser," Opt. Lett. **43**, 2225–2228 (2018).

[145]M. Wienold, T. Alam, L. Schrottke, H. Grahn, and H.-W. Hübers, "Doppler-free spectroscopy with a terahertz quantum-cascade laser," Opt. Express **26**, 6692–6699 (2018).

[146]Y. J. Han, J. Partington, R. Chhantyal-Pun, M. Henry, O. Auriacombe, T. Rawlings, L. H. Li, J. Keeley, M. Oldfield, N. Brewster, R. Dong, P. Dean, A. G. Davies, B. N. Ellison, E. H. Linfield, and A. Valavanis, "Gas spectroscopy through multimode self-mixing in a double-metal terahertz quantum cascade laser," Opt. Lett. **43**, 5933–5936 (2018).

[147]J. Morville, D. Romanini, and E. Kerstel, "Cavity enhanced absorption spectroscopy with optical feedback," in *Cavity-Enhanced Spectroscopy and Sensing* (Springer, 2014), Chap. 5, pp. 163–209.

[148]J. Burkart, D. Romanini, and S. Kassi, "Optical feedback stabilized laser tuned by single-sideband modulation," Opt. Lett. **38**, 2062–2064 (2013).

[149]R. Braakman and G. A. Blake, "Principles and promise of fabry–perot resonators at terahertz frequencies," J. Appl. Phys. **109**, 063102 (2011).

[150]L. Consolino, A. Campa, D. Mazzotti, M. S. Vitiello, P. De Natale, and S. Bartalini, "Bow-tie cavity for terahertz radiation," Photonics **6**, 1 (2019).

[151]I. Ventrillard, P. Gorrotxategi-Carbajo, and D. Romanini, "Part per trillion nitric oxide measurement by optical feedback cavity-enhanced absorption spectroscopy in the mid-infrared," Appl. Phys. B **123**, 180 (2017).

[152]Y. L. Lim, K. Bertling, T. Taimre, G. Agnew, P. Dean, D. Indjin, Y. Han, L. Li, E. H. Linfield, A. G. Davies, A. Robinson, T. Gillespie, C. Glenn, and A. D. Rakić, "Pulsed-mode laser feedback interferometry: A new technique for imaging using THz QCLs," in 8th International Quantum Cascade Lasers School & Workshop IQCLSW 2018, Cassis, France, 2–7 September 2018 (2018).

[153]Y. L. Lim, K. Bertling, T. Taimre, T. Gillespie, C. Glenn, A. Robinson, D. Indjin, Y. Han, L. Li, E. H. Linfield, A. G. Davies, P. Dean, and A. D. Rakić,

"Coherent imaging using laser feedback interferometry with pulsed-mode terahertz quantum cascade lasers," Opt. Express **27**, 10221–10233 (2019).

[154]S. Adachi, *Optical Properties of Crystalline and Amorphous Semiconductors: Materials and Fundamental Principles* (Springer, New York, 1999).

[155]K. Ohtani, M. Beck, M. J. Suess, J. Faist, A. M. Andrews, T. Zederbauer, H. Detz, W. Schrenk, and G. Strasser, "Far-infrared quantum cascade lasers operating in the AIAs phonon Reststrahlen band," ACS Photonics **3**, 2280–2284 (2016).

[156]H. Detz, A. M. Andrews, M. A. Kainz, S. Schönhuber, T. Zederbauer, D. MacFarland, M. Krall, C. Deutsch, M. Brandstetter, P. Klang, W. Schrenk, K. Unterrainer, and G. Strasser, "Evaluation of material systems for THz quantum cascade laser active regions," Phys. Status Solidi A **216**, 1800504 (2018).